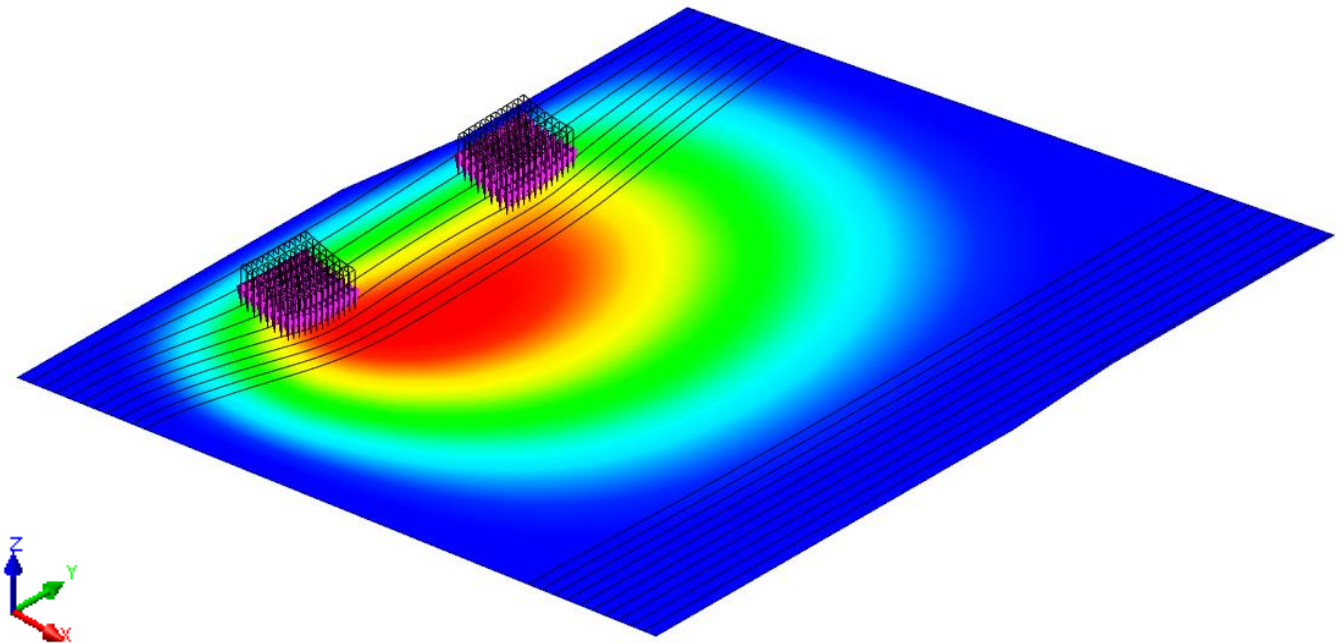




**CHALMERS**  
UNIVERSITY OF TECHNOLOGY

---



# **Assessment of Punching Capacity of RC Bridge Deck Slab in Kiruna**

## **Finite element modelling of RC slab**

Master's Thesis in the Master's Programme Structural Engineering and Building Performance Design

MARCO KOBLER



MASTER'S THESIS BOMX02-16-95

# Assessment of Punching Capacity of RC Bridge Deck Slab in Kiruna

Finite element modelling of RC slab

*Master's Thesis in the Master's Programme Structural Engineering and Building Performance  
Design*

MARCO KOBLER

Department of Civil and Environmental Engineering

*Division of Structural Engineering*

Concrete Structures

CHALMERS UNIVERSITY OF TECHNOLOGY

Göteborg, Sweden 2016



Assessment of Punching Capacity of RC Bridge Deck Slab in Kiruna  
Finite element modelling of RC slab

*Master's Thesis in the Master's Programme Structural Engineering and Building  
Performance Design*

MARCO KOBLER

© MARCO KOBLER, 2016

Examensarbete BOMX02-16-95/ Institutionen för bygg- och miljöteknik,  
Chalmers tekniska högskola, 2016

Department of Civil and Environmental Engineering  
Division of Structural Engineering  
Concrete Structures  
Chalmers University of Technology  
SE-412 96 Göteborg  
Sweden  
Telephone: + 46 (0)31-772 1000

Cover:

Displacement of a simply supported slab; structural nonlinear; load-controlled method;  
total applied load 3680 kN

Printed by Chalmers Reproservice, Göteborg, Sweden, 2016



# Assessment of Punching Capacity of RC Bridge Deck Slab in Kiruna

## Finite element modelling of RC slab

*Master's thesis in the Master's Programme Structural Engineering and Building Performance Design*

MARCO KOBLER

Department of Civil and Environmental Engineering  
Division of Structural Engineering  
Concrete Structures  
Chalmers University of Technology

## ABSTRACT

Subject of this master's thesis was a 55-year old pre-stressed concrete bridge in Kiruna. The five-span girder bridge with a length of 121 m contained three main beams which were cast together with the bridge deck slab. In order to assess the shear and punching resistance of the slab, it was loaded to failure by two concentrated load plates, which simulate vehicle wheels. Based on these testing results, with a recently developed method, the assessment of the punching capacity shall be improved.

The aim of this master's thesis was to calibrate more accurate predictions of the response and capacity of bridge deck slabs subjected to concentrated loads. Therefore, the load-carrying capacity of the bridge deck slab was estimated according to a multi-level assessment strategy developed by Plos *et al.* (2015). The strategy is based on the principle of successively improved evaluation in structural assessment. On initial level, the aim is to obtain fast results, mostly based on standards. If safety cannot be assured, more advanced analysis methods have to be performed. Thus, Level II & III assessments are performed with 3D finite element models. Especially non-linear analysis takes into account the structural response of reinforced concrete in a realistic way. On each level, the failure modes for punching, one-way shear and flexural resistance were estimated.

It was shown that simplified methods underestimate structural supply because they do not account additional mechanism. Thus, the application of non-linear FE models is crucial in order to achieve more accurate predictions due to additional material information. The results show that more advanced methods yield to higher, yet conservative, predictions of the capacity.

Regarding parameter study it could be concluded that a variation of the effective depth did not have a big influence on the punching capacity. On the other hand, by analysing the influence of boundary conditions, it was shown that in the current situation a fully fixed slab delivered an approximately 50 % higher load carrying capacity.

**Keywords:** Punching shear capacity, finite element methods, bridge deck slab, multi-level assessment, full-scale test





# Contents

1	INTRODUCTION	1
1.1	Background	1
1.2	Aim	1
1.3	Method	2
1.4	Limitations of the project	2
2	LITERATURE STUDY	3
2.1	Kiruna Bridge	3
2.2	Multi-level assessment strategy	7
2.3	Critical shear crack theory (CSCT)	10
3	MULTI-LEVEL STRUCTURAL ANALYSIS	12
3.1	Level I: Hand-calculations	13
3.2	Level II: Linear analyses	19
3.3	Level III: Non-linear analyses	29
3.4	Results and discussion	38
4	PARAMETER STUDY	41
4.1	Influence of boundary conditions	41
4.2	Influence of effective depth	50
5	CONCLUSIONS	52
6	FUTURE STUDY	54
7	REFERENCES	55



# Preface

The thesis investigates the punching shear capacity of existing bridge deck slabs. It was carried out at the Division of Structural Engineering, Concrete Structures, Department of Civil and Environmental Engineering, Chalmers University of Technology, Sweden. The work on this thesis was started in February 2016 and ended in June 2016.

This study is part of an ongoing research project concerning structural assessment of existing bridge deck slabs. The overall project called "Load Carrying Capacity of Existing Bridge Deck Slabs" was initiated in 2012 and is planned to be finished at the end of 2016. The project is mainly financed through Trafikverket.

Based on tests carried out on a reinforced concrete bridge in Kiruna, in this master's thesis the punching capacity of the bridge deck slab shall be assessed with analytical and numerical calculations. It is expected to lead to improved methods for design and assessment of bridge deck slabs. A parametric study was performed in order to evaluate the impact of parameters on the final result.

The thesis has been carried out with researcher Kamyab Zandi as examiner and PhD Student Jiangpeng Shu as supervisor. I greatly appreciate their guidance, support and encouragement. Especially, a big thank to Jiangpeng who supported my thesis in a great way and always took time for fruitful discussions. I also want to thank Associate Professor Mario Plos who acted as my examiner at the beginning. Since Mario was on sick leave, for the second part of my thesis Kamyab continued as my examiner and did thereby a great job.

Göteborg June 2016

Marco Kobler

# Notations

## Roman upper case letters

$A_c$	Cross sectional area of concrete
$A_s$	Cross sectional area of steel reinforcement
$C_{Rd,c}$	Coefficient including concrete partial safety factor
$E_{cm}$	Young modulus of concrete
$E_s$	Young modulus of steel reinforcement
$L_x, L_y$	Length of the span / Length of the yield line
$Q$	Applied Load
$V_{Ed}$	Design shear force value
$V_{perp,d,max}$	Maximum shear force per unit length perpendicular to the basic control perimeter
$V_{Rd,c}$	Design shear resistance

## Roman lower case letters

$b_0$	Shear-resisting control perimeter
$b_1$	Basic control perimeter
$b_w$	Slab width of the cross section
$c$	Cover of reinforcement
$d$	Effective depth of the slab
$d_g$	Maximum size of the aggregate
$d_{g0}$	Reference size equal to 16 mm
$d_v$	Shear-resisting effective depth of the slab
$f_{ck}$	Characteristic concrete compressive strength
$f_{cm}$	Average concrete compressive strength
$f_{sm}$	Average steel yield strength
$f_{yd}$	Design yield strength of steel
$f_{yk}$	Characteristic yield strength of steel
$k$	Factor to account for size effects
$k_{dg}$	Factor depending on the maximum size of the aggregate
$k_e$	Coefficient of eccentricity
$k_v$	Coefficient for determining the one-way shear resistance
$k_\psi$	Coefficient of rotations

$m_{Ed}$	Average bending moment acting in the support strip
$m_{Rd}$	Moment resistance per meter
$r_s$	Distance from the loading area to the position where the radial bending moment is zero
$u$	Control perimeter
$v_{Rd,c}$	Shear resistance
$v_{min}$	Minimal shear resistance
$z$	Distance between top and bottom reinforcement

### **Greek letters**

$\beta$	Reducing factor for loads close to the point loads
$\gamma_c$	Partial safety factor for concrete
$\delta$	Vertical displacement due to applied load
$\theta$	Rotation of the yield line
$\nu$	Poisson's ratio
$\rho$	Reinforcement ratio
$\rho_c$	Mass density of concrete
$\rho_s$	Mass density of the reinforcement
$\sigma_{cp}$	Concrete pre-stressing stress
$\psi$	Rotation of slab outside the loading points



# 1 Introduction

## 1.1 Background

Bridges are an important part of our infrastructure and are essential for the transportation of goods and people. Thereby they are delivered a heavy wear due to continuously increasing traffic loads as well as nature's influence. Thus, either by constructing or by maintenance it is essential to know the behaviour of the bridge in a high grade of accuracy. In particular for existing bridges strengthening or even replacement is connected with spending a massive amount of money. Thus, to avoid these interventions, more accurate models for assessment of existing bridges have to be calibrated. Since bridge deck slabs are often critical for load carrying capacity, this thesis focuses on this member.

By testing a 55-year old pre-stressed reinforced concrete bridge to failure, the punching shear resistance of the deck slab was tested. Based on this outcome, the capacity of the bridge deck slab should be estimated with different methods at different levels of accuracy. Therefore, a multi-level assessment strategy developed by Plos *et al.* (2015) was applied. Finally, a parameter study was performed to assess the influence of several important parameters on the calculated punching capacity.

In this master's thesis the influence of the boundary conditions was analysed more in detail. In particular the differences which result by assuming a simply supported slab or in contrast a fully fixed slab.

## 1.2 Aim

The aim of this master's thesis was to assess the punching capacity of existing bridge deck slabs with appropriate finite element (FE) models and consequently to be able to provide more accurate predictions. In addition, hand-calculations were compared with linear and finally non-linear analyses.

The objectives are summarized below:

- Comparison between analytical calculations, numerical analyses and test results according to a multi-level structural assessment strategy.
- Understanding of the influence of different parameters, such as boundary conditions, effective depth and control perimeter.
- Developing a suggestion for improved analytical and FE-method for engineering practice.
- Providing more accurate predictions of the response and punching capacity of bridge deck slabs.

### 1.3 Method

The analyses were done based on the scheme for multi-level assessment of reinforced concrete bridge deck slabs (Plos et al., 2015). This allows structural analyses on different levels of detailing. For Level I assessment simplified analyses methods as Eurocode 2 (EN 1992-1-1, 2004) or Model Code (CEB-FIP, 2013) were used. More accurate predictions were achieved with FE-software DIANA. Linear (Level II) and finally non-linear (Level III) calculations led to an enhanced assessment. The grade of accuracy could have been increased with Level IV and Level V analyses methods; these however were not part of this thesis. Nevertheless, in most cases the punching resistance of existing bridge deck slabs is much higher than the calculated results. Concerning to this fact a suggestion for improved analysis method should be developed. This could be reached for instance by varying the boundary conditions, the effective depth or by replacing the basic control perimeter by the shear-resisting perimeter according to Model code (CEB-FIP, 2013).

### 1.4 Limitations of the project

In contrast to the full-scale failure test which was performed, in the FE analysis only the exposed part of the bridge was investigated. For the residual part of the bridge appropriate boundary conditions were chosen. Furthermore, in this thesis according to the multi-level assessment strategy only Level I to III analyses had been performed. This means that more detailed continuum elements, such as solid elements were not applied. Instead 2D shell elements were used, which are not able to describe out-of-plane shear, punching or anchorage failure (Plos et al., 2015). Thus, the critical shear crack theory of Muttoni had been applied in order to determine the punching capacity. Regarding this theory only slabs without transversal reinforcement had been analysed.

In addition, when creating a non-linear FE model many structural parameters such as element type, boundary conditions or material model had to be chosen. All of these input parameters were connected to uncertainties which ultimately may affect the result. Also for the computation process, parameters such as mesh density, element interpolation function or integration schemes may have an influence on the result, none of which were studied in this work.



## 2 Literature Study

Full-scale tests are seldom performed due to high costs and lack of test objects. Thus, most experiments are carried out in experiment halls. Therefore, only a limited part of the whole structure can be rebuilt and consequently it is necessary to specify several simplifications.

### 2.1 Kiruna Bridge

The Kiruna Bridge, constructed in 1959, was located in northern Sweden and was closed due to seismic activities based on underground mining. As a result the bridge became an object for experimental studies. To assess the load-carrying capacity both non-destructive and destructive test procedures were performed. The focus of this study lied on a full-scale failure test of the bridge slab.

#### 2.1.1 Situation

Three longitudinal girders connected by the bridge deck slab and cross beams built the superstructure. For the punching test the second span with a total length of 20.5 m was investigated. As shown in Bagge (2014), two load plates 350 mm x 600 mm spaced 2.0 m apart were applied. Linked with a force controlled hydraulic jack the load was raised up to failure.

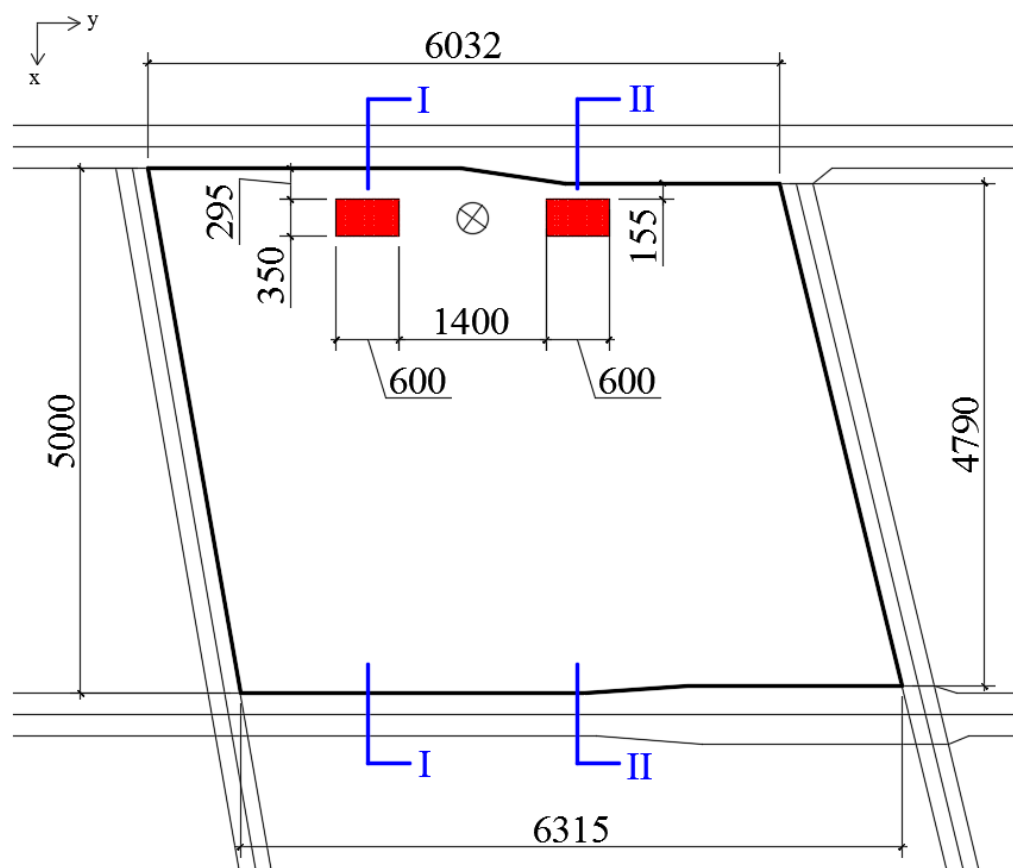


Figure 1: Bridge deck slab including loading points and location of cross sections (blue marked); all dimensions are in mm.

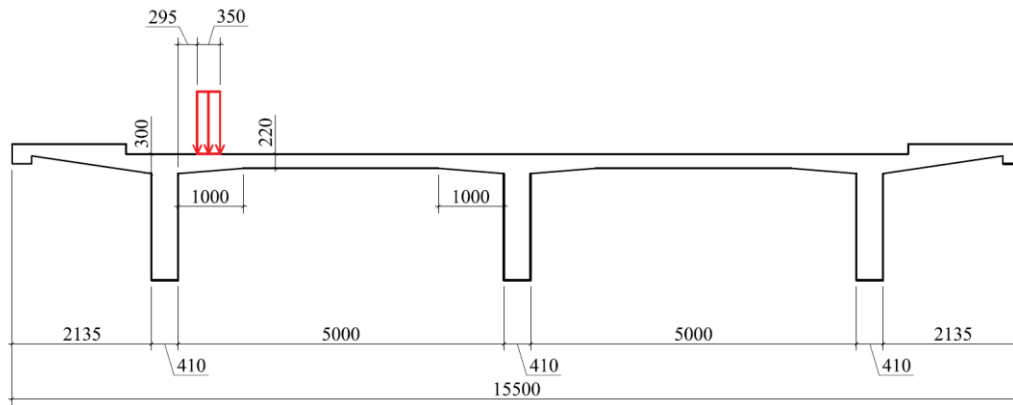


Figure 2: Cross section I including further loading point; all dimensions are in mm.

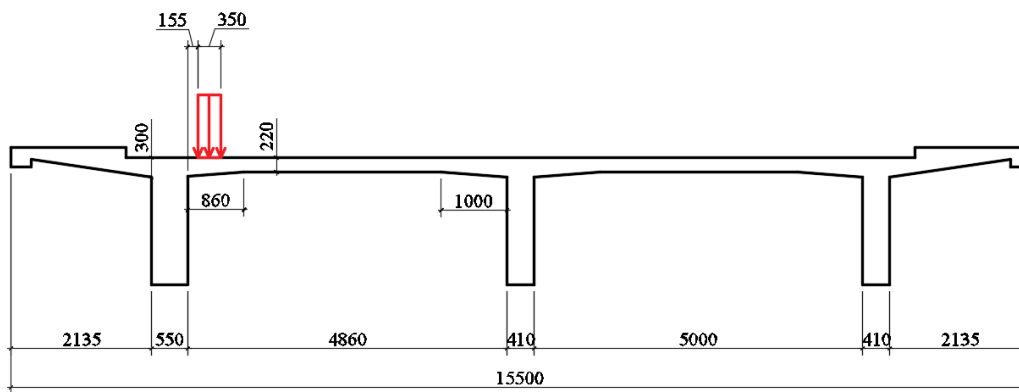


Figure 3: Cross section II including closer loading point; all dimensions are in mm.

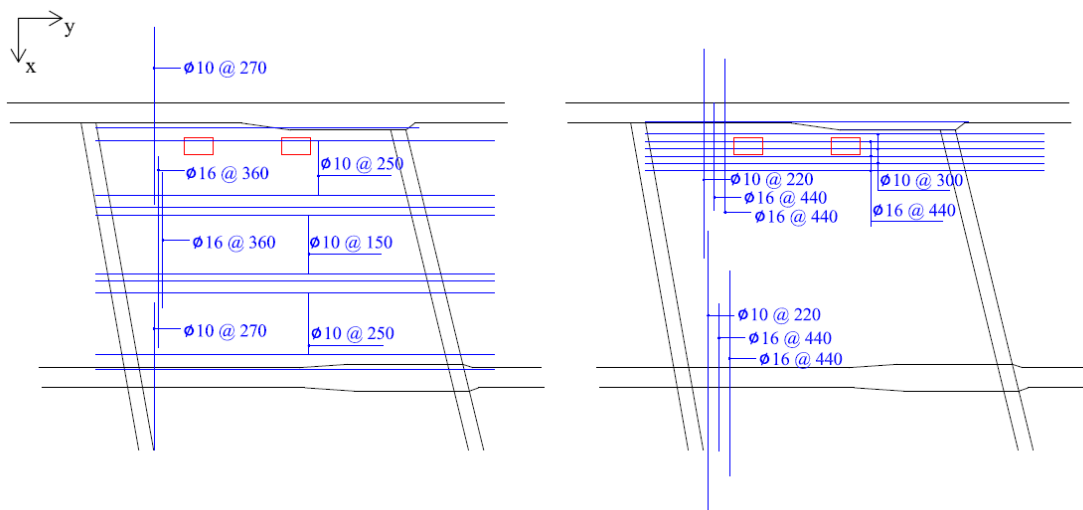


Figure 4: Bottom reinforcement ratio 0.55 % (left) and top reinforcement ratio 0.84 % (right); all dimensions are in mm.

### 2.1.2 Material properties

Material parameters were determined through tests. Table 1 shows an overview of the measured in-situ material properties (Bagge et al., 2015). These are mean values excluding partial safety factors.

Table 1: Measured in-situ material parameters.

Concrete	
Concrete compressive strength	$f_{cm} = 62.2 \text{ MPa}$
Concrete tensile strength	$f_{ctm} = 4.2 \text{ MPa}$
Young modulus of concrete	$E_{cm} = 38.1 \text{ GPa}$
Mass density	$\rho_c = 2500 \text{ kg/m}^3$
Poisson's ratio concrete	$\nu_c = 0.2$
Reinforcement	
Yield strength transverse direction	$f_{sm,t} = 584 \text{ MPa}$
Yield strength longitudinal direction	$f_{sm,l} = 667 \text{ MPa}$
Young modulus of steel reinforcement	$E_s = 200 \text{ GPa}$
Mass density	$\rho_s = 7850 \text{ kg/m}^3$
Poisson's ratio steel	$\nu_s = 0.3$

Material properties used in standards are given at the design level. However, for calibrating models which should describe the reality as realistic as possible material properties excluding partial safety factors are more useful. Therefore, the equations proposed in standards were calculated deducting partial safety factors and by replacing the characteristic in-situ concrete strength by the corresponding average value.

### 2.1.3 Testing results

A comparison between test results and analytical analysis based on Eurocode 2 (EN 1992-1-1, 2004) had been carried out in Bagge *et al.* (2015). All in all, the experimental outcome was much higher compared to the analytical analysis. Whereas in the full-scale test a total punching capacity of 3320 kN (1660 kN for each loading plate) was measured, simplified calculations based on Eurocode 2 (EN 1992-1-1, 2004) resulted in a punching capacity of 840 kN (excluding partial safety factors) per loading plate. Thus, within the scope of this thesis more advanced methods were applied. Especially non-linear finite element analyses were performed to estimate the punching capacity in a higher grade of accuracy.



Figure 5: Bottom view of the slab showing the location of the loading points.



Figure 6: Devices installed above the slab: Closer loading area and stiff steel beam which connected the two loading plates (left) and hydraulic jack (right).



Figure 7: Bottom view of the slab showing punching failure occurred at the further loading plate.

## 2.2 Multi-level assessment strategy

In Plos *et al.* (2015) a multi-level assessment scheme for reinforced concrete bridge deck slabs is proposed. Thereby starting with simplified calculations, the grade of complexity as well as the grade of accuracy is raised. However, according to Plos *et al.* (2015) in all levels the recommendations are believed to be conservative.

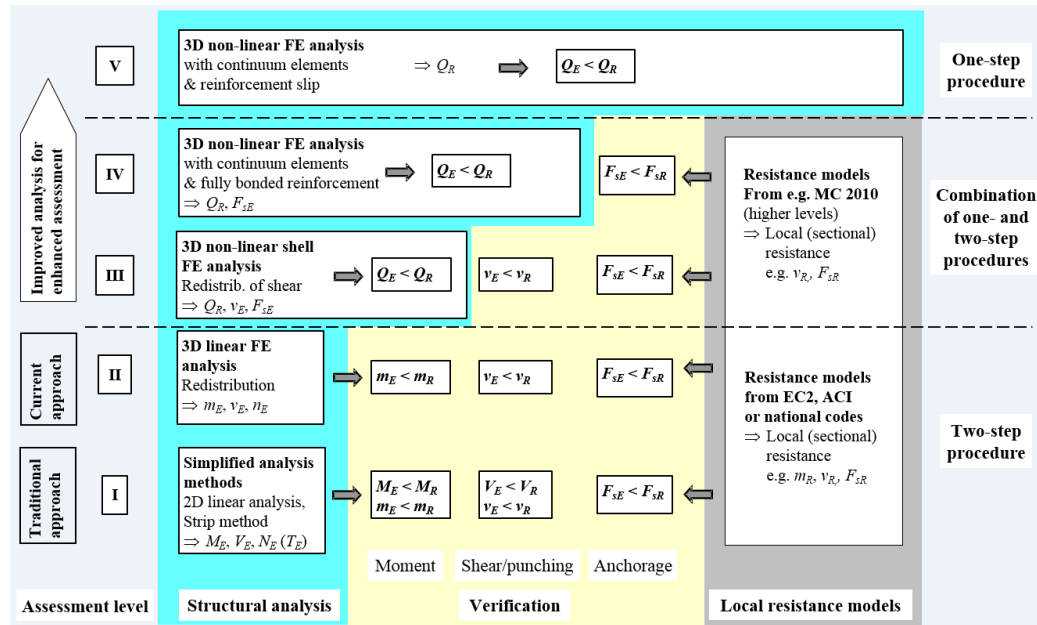


Figure 8: Scheme for multi-level assessment of reinforced concrete bridge deck slabs (Plos *et al.*, 2015).

Within the scope of this thesis Level I - III analyses had been carried out. While Level I & II assume a linear material behaviour, Level III is based on non-linearity.

On initial level, the aim is to obtain fast results, mostly based on standards. Therefore, the structure's properties as well as the modelling according to drawings. If safety cannot be assured more specific information is necessary, e.g. by doing material tests, carrying out an inspection or by performing more advanced analysis methods (Plos *et al.*, 2015). Level II & III assessments are performed with 3D finite element models, using shell elements. Especially non-linear analyses take into account the structural response of reinforced concrete in a realistic way. Thus, concrete cracking, reinforcement yielding but also the influence of the interaction between concrete and reinforcement is included.

More advanced methods at Level IV & V can be performed with solid elements, with an improved understanding of the structure presupposes.

## 2.2.1 Punching assessment

In order to obtain the punching capacity there exist several levels of accuracy. Whereas in Eurocode 2 (EN 1992-1-1, 2004) only one formula is given, in Model code (CEB-FIP, 2013) in total eight combinations exist, differing in the grade of complexity. This follows, since in Model code (CEB-FIP, 2013) the rotation  $\psi$  as well as the control perimeter  $b$  can be specified. Table 2 shows all combinations, starting with simplified Level I calculations up to non-linear analyses.

For Level III analyses, instead of using the rotation  $\psi_{IV}$  and the control perimeter, the critical shear crack theory of Muttoni (Chapter 2.3) was applied.

Table 2: Assessment levels listed in left column as well as associated approximation for the rotation perimeter  $\psi$  (middle column) and for the control perimeter (right column) based on Model code (CEB-FIP, 2013).

Level	Rotation $\psi$	Control perimeter $b$
III	IV	$b_0$
	IV	$b_1$
II	III	$b_0$
	III	$b_1$
	II	$b_0$
	II	$b_1$
	I	$b_0$
I	I	$b_1$

### Rotation $\psi$ around the supported area based on Model code (CEB-FIP, 2013)

Level I approximation:  $\psi_I = 1.5 \frac{r_s}{d} \frac{f_{yd}}{E_s}$

Level II approximation:  $\psi_{II} = 1.5 \frac{r_s}{d} \frac{f_{yd}}{E_s} \left( \frac{m_{Ed}}{m_{Rd}} \right)^{1.5}$

Level III approximation:  $\psi_{III} = 1.2 \frac{r_s}{d} \frac{f_{yd}}{E_s} \left( \frac{m_{Ed}}{m_{Rd}} \right)^{1.5}$  (uncracked FEM)

Level IV approximation:  $\psi_{IV}$  is calculated on the basis of a non-linear analysis

### Control perimeter $b$ based on Model code (CEB-FIP, 2013)

Basic control perimeter:  $b_1$

Shear-resisting control perimeter:  $b_0 = \frac{V_{Ed}}{V_{perp,d,max}}$

### 2.2.2 One-way shear assessment

Since the two loading plates were placed close to the outside girder, the main part of the resulting shear force was carried by this support. For this phenomenon, called one-way shear, along a critical section the whole shear force has to be absorbed. In order to get the effective width at the critical section in Model code (CEB-FIP, 2013) it is proposed to take a distribution angle of  $60^\circ$  if the slab is assumed to be simply supported. In Eurocode 2 (EN 1992-1-1, 2004) on the other hand, there is neither the distribution angle nor the location of the critical section defined. Thus, a distribution angle of  $45^\circ$  was assumed and the width of the critical section was determined by the head of the support.

For Level II analysis more specific calculations based on the Swedish recommendation in Pacoste *et al.* (2012) were performed to obtain the critical section and the effective width. Further, a random load was applied on the linear FE model in order to get the average shear distribution along the critical width. Due to linear material properties in Level II analysis and on the basis of the maximum shear force from Level I assessment, the maximal one-way shear resistance could be determined.

For Level III calculations there exists no known method which yields more accurate results than Level II analysis.

### 2.2.3 Flexure assessment

In order to determine the flexural resistance, for Level I analysis the yield-line method was used. In accordance to determine the maximal loading capacity the energy conservation principle was applied.

For Level II analysis, similar to one-way shear, the critical section as well as the critical width were provided according to Pacoste *et al.* (2012). With the outputted average moment distribution along the critical section and the maximal flexural resistance from Level I, the bending resistance from Level II could be gained. Therefore also the linear material behaviour was used.

For Level III assessment, the flexural resistance was equal to the maximum load which was added in the FE model just before failure occurred. This was possible since with shell elements bending failure can be reflected (Plos *et al.*, 2015).

## 2.3 Critical shear crack theory (CSCT)

Flat slabs and especially slabs without transverse reinforcement are prevalent because of their simplicity as well as for their low construction costs. On the other hand, they are also very critical particularly for punching failure and that is why they are often the object for experiments (Muttoni, 2008). The most common theory for evaluating the punching shear resistance of flat slabs without reinforcement was developed by Aurelio Muttoni, a Swiss civil engineer. On the basis of the opening of a critical shear crack, it analyses the rotation of the slab around a supported area due to an applied load. This method, called critical shear crack theory (CSCT), served as basis for several design codes, such as Model code.

The application of this method was published in 2008 in Muttoni (2008). The main content is summarized in this chapter.

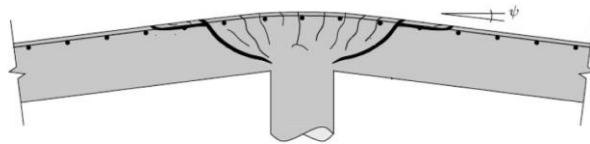


Figure 9: Rotation of a slab, adopted from Model code (CEB-FIP, 2013).

The effective punching capacity results at the point where the load-rotation curve of the slab crosses the failure criterion curve (Point A in Figure 10). Thus, to obtain the exact punching resistance equation (1) and (2) have to be set equally.

$$\text{Failure criterion: } \frac{V_R}{b_0 d \sqrt{f_c}} = \frac{3/4}{1 + 15 \frac{\psi d}{d_{g0} + d_g}} \quad (1)$$

$$\text{Load-rotation curve: } \psi = 1.5 \frac{r_s f_y}{d E_s} \left( \frac{V}{V_{flex}} \right)^{1.5} \quad (2)$$

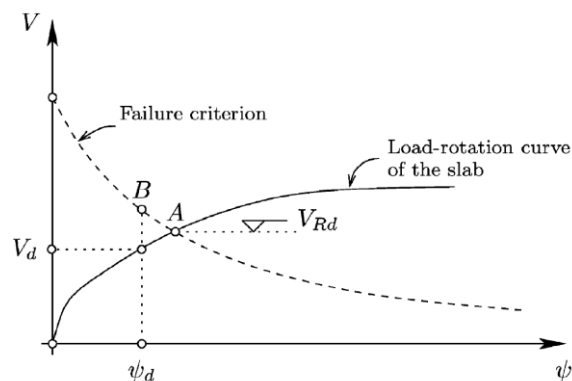


Figure 10: Approach to determine the punching strength of the slab, adopted from Muttoni (2008).



Both, equation (1) and (2) can be found in a slightly rearranged form in Model code (CEB-FIP, 2013). Whereas equation (1) expresses the design shear resistance, equation (2) describes the rotation.

Table 3: Comparison between Muttoni and Model code (CEB-FIP, 2013).

Muttoni (2008)	Model code (2010)
$\frac{V_R}{b_0 d \sqrt{f_c}} = \frac{3/4}{1 + 15 \frac{\psi d}{d_{g0} + d_g}} \quad (1)$	$V_{Rd,c} = k_\psi \frac{\sqrt{f_{ck}}}{\gamma_c} b_0 d_v$ $k_\psi = \frac{1}{1.5 + 0.9 k_{dg} \psi d}$ $k_{dg} = \frac{32}{d_{g0} + d_g}$
$\psi = 1.5 \frac{r_s f_y}{d E_s} \left( \frac{V}{V_{flex}} \right)^{1.5} \quad (2)$ $V_{flex} \cong 8 m_{Rd}$	$\psi_{II} = 1.5 \frac{r_s f_y}{d E_s} \left( \frac{m_{Ed}}{m_{Rd}} \right)^{1.5}$ $m_{Ed} = V_{Ed} \left( \frac{1}{8} + fct(e_{u,i}) \right)$

Therefore;

- Since the rotation is slenderness-dependant, it is inversely proportional to the thickness of the slab. This conclusion follows after introducing equation (2) into equation (1), the slab thickness  $d$  cancels on the right-hand side of the equation.
- According to Muttoni (2008) the punching shear strength of a slab is depending more on the span of the slab than on the thickness.
- The amount of shear that can be transferred across the critical shear crack depends on the roughness of the crack. Therefore the nominal crack width  $\psi d$  is divided by a function considering the aggregate size.
- The width of the critical crack can be assumed to be proportional to the product  $\psi d$  (Muttoni, 2008).
- The thicker a slab is, the more it loses its ductility and acts more brittle. Thus, according to Muttoni (2008), for thick slabs the only way to get ductility is to place punching reinforcement.

### 3 Multi-level Structural Analysis

Figure 11 shows the methods which were applied in this master's thesis for the multi-level assessment strategy. Starting with simplified calculations in Level I (Chapter 3.1), in Level II linear structural analyses (Chapter 3.2) and finally in Level III non-linear FE analyses (Chapter 3.3) were performed. Thereby, punching, one-way shear and bending were assessed.

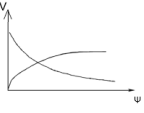
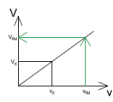
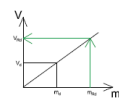
	Punching	One-way shear	Flexure
Level III		—	Failure point (shell elements)
Level II	MC		
Level I	EC 2 MC	EC 2 MC	Yield line method

Figure 11: Overview of the applied methods in this master's thesis.

#### Introductory remarks and assumptions:

- Since the two loading points were placed in different distances from the support, in the further report they are named as “closer load” meaning the load closer to the support and “further load” for the one which is located further from the support.
- All calculations had been performed without safety factors. Thus, the equations from standards were applied after deducting partial safety factors. In this way it was possible to compare the results from numerical analyses with hand-calculations and test results.
- Since the reinforcement and the effective cover were not clearly defined, for the effective depth always the approximation  $d \approx 0.85 t$  was used.
- For boundary conditions in longitudinal direction it was assumed that the edges were fully fixed since the slab continues over several spans. On the other hand, in transversal direction three longitudinal girders represented the supports. Thus for the boundary in the middle it was assumed that the slab was fixed, since bending moments used to be equally between a fixed one span beam and the support in the middle of a two-span-beam. On the other hand, as shown in Chapter 2.1.1, a massive cantilever followed next to the outside girder. Simply calculations delivered though, that the own weight of this cantilever came to less than 10 kN/m, why it could be neglected compared to a final test load of 1660 kN.

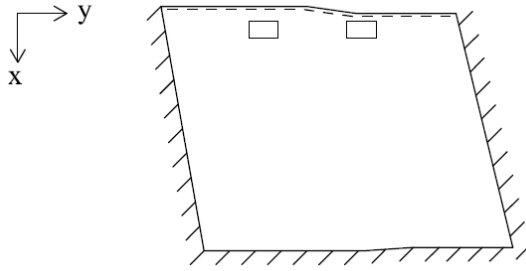
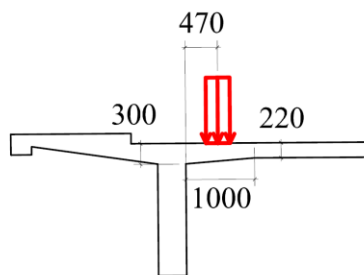


Figure 12: Assumed boundary conditions of the slab.

### 3.1 Level I: Hand-calculations

In a first step simplified analyses had been carried out according to Eurocode 2 (EN 1992-1-1, 2004) and Model code (CEB-FIP, 2013).

#### 3.1.1 Punching shear resistance



$$t = 300 - \frac{300 - 220}{1000} 470 = 262 \text{ mm}$$

Figure 13: Cross section showing location of the added load (left) and the thickness of the slab below the loading point (right); all dimensions are in mm.

The thickness of the slab below the loading plates followed to  $t = 262 \text{ mm}$  and the effective depth was assumed to be  $d \cong 0.85 t = 223 \text{ mm}$ .

##### 3.1.1.1 Eurocode 2

Generally, the punching shear resistance is calculated as the shear force per square meter along a control perimeter times the effective depth.

$$V_{Rd,c} = v_{Rd,c} u d \quad (3)$$

The shear capacity will be determined for a specified control perimeter  $u$  at a distance of twice the effective depth from the cross section ( $2d$ ), see Figure 14.

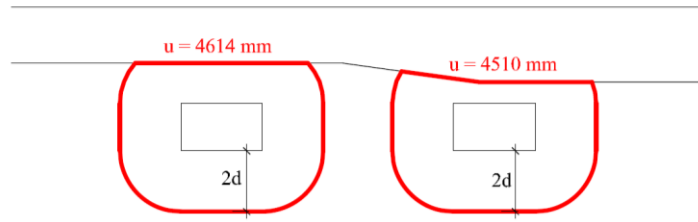


Figure 14: Control perimeter according to Eurocode 2 (EN 1992-1-1, 2004).

For load areas of 600 mm x 350 mm and an average effective depth of 223 mm, a decisive control perimeter of 4.51 m resulted. Since there was no compressive stress in concrete due to axial load or pre-stressing, the equation for the punching shear resistance of slabs without shear reinforcement was applied.

$$v_{Rd,c} = 0.18 k (100\rho_l f_{cm})^{1/3} \quad (4)$$

Where  $k$  is a factor dependent on the effective depth of the slab,  $\rho_l$  denotes the reinforcement ratio and  $f_{cm}$  the average concrete compressive strength.

A minimum shear strength depending on the effective depth as well as the compressive strength of concrete is given in equation (5).

$$v_{min} = 0.035 k^{3/2} f_{cm}^{1/2} \quad (5)$$

Finally, an average punching capacity of 754 kN for the closer and 772 kN for the further load resulted. More detailed calculations can be found in Appendix B1.

### 3.1.1.2 Model code

The punching shear resistance is calculated as the shear per square meter along a control perimeter times the effective depth.

$$V_{Rd,c} = v_{Rd,c} b_1 d_v \quad (6)$$

The basic control perimeter  $b_1$  is measured in a distance of  $d_v/2$  from the supported area and resulted to 2.60 m.

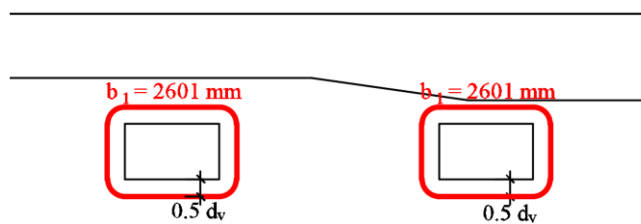


Figure 15: Control perimeter according to Model code (CEB-FIP, 2013).

The punching shear resistance of slabs bases without shear reinforcement is calculated as shown in equations (7) to (9) and has to be done for each direction separately.

$$v_{RC,c} = k_{\psi} \sqrt{f_{cm}} \quad (7)$$

$$k_{\psi} = \frac{1}{1.5 + 0.9 k_{dg} \psi d} \quad (8)$$

$$\psi_I = 1.5 \frac{r_s f_{yd}}{d E_s} \quad (9)$$

The parameter  $k_{\psi}$  is a function of plate rotation, member size and maximum grain. The maximum size of aggregate particles was assumed to be 16 mm and consequently  $k_{dg}$  resulted to 1.0.

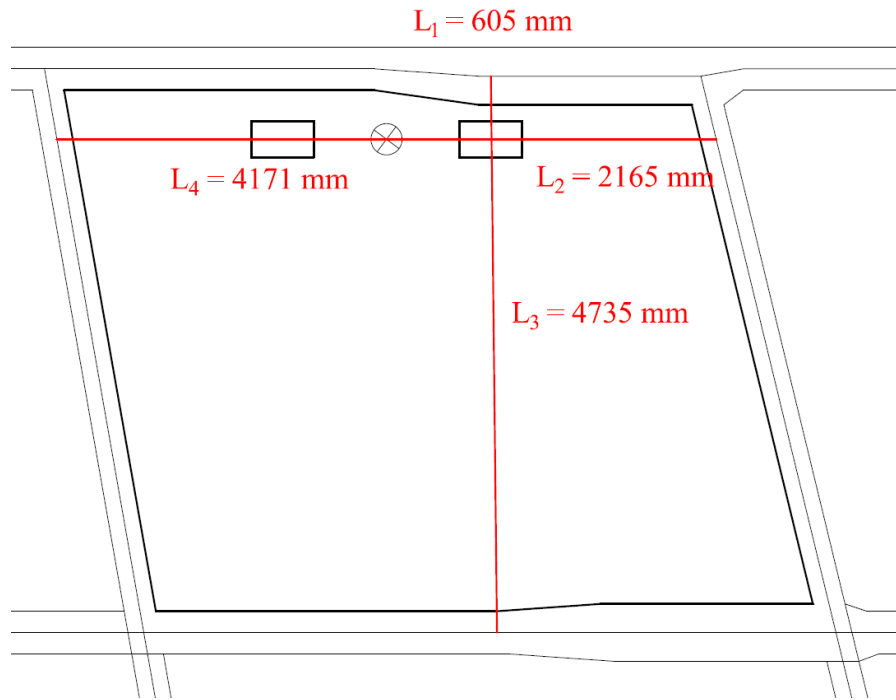


Figure 16: Length of the spans (closer load).

In Model code (CEB-FIP, 2013) it is proposed that the distance from the loading area to the position where the radial bending moment is zero may be assumed as  $r_s = 0.22 L$ . However, it is also mentioned that this assumption is only valid for regular slabs where the ratio of the spans  $L_x/L_y$  is in between 0.5 and 2.0. Although in the present case this condition was not fulfilled, calculations were performed, see also Appendix B2.

Thereby a punching capacity of 812 kN resulted.

### 3.1.2 One-way shear resistance

#### 3.1.2.1 Eurocode 2

For members not requiring design shear reinforcement, the value for the shear resistance follows out of equation (10).

$$V_{Rd,c} = v_{Rd,c} b_w d \quad (10)$$

Since there is no recommendation in Eurocode 2 (EN 1992-1-1, 2004) for determining the distribution width  $b_w$  due to a point load, for Level I calculation it was assumed that the distribution width formed an angle of  $45^\circ$  with the applied point load.

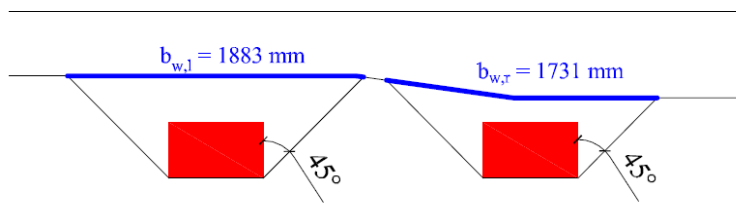


Figure 17: Width of the critical section by the head of the support.

The one-way shear resistance was gained according to Eurocode 2 (EN 1992-1-1, 2004) as shown in equation (11).

$$v_{Rd,c} = 0.18 k (100 \rho_t f_{cm})^{1/3} \quad (11)$$

The equation looks exactly equal to equation (4), which was used to determine the punching shear resistance, but with the difference that the reinforcement ratio takes only the tensile reinforcement of the shear direction into account.

In summary, one-way shear resistance followed to 477 kN for the further load and to 439 kN for the closer load.

For detailed calculations, see Appendix B3.

#### 3.1.2.2 Model code

For members not requiring design shear reinforcement, the value for the shear resistance follows out of equations (12) to (14).

$$V_{Rd,c} = v_{Rd,c} b_w z \quad (12)$$

$$v_{Rd,c} = k_v \sqrt{f_{cm}} \quad (13)$$

$$k_v = \frac{180}{1000 + 1.25z} \quad (14)$$

The critical width was calculated according to Model code (CEB-FIP, 2013) and was taken at the lesser of the distances equal to  $d$  and  $a_v/2$  from the face of the support. If assuming a clamped slab the load distribution angle should be taken as  $\alpha = 60^\circ$  according to Model code (CEB-FIP, 2013).

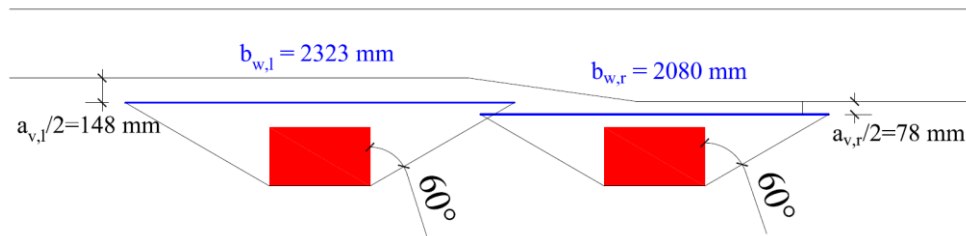


Figure 18: Locations of the critical sections and critical widths according to Model code (CEB-FIP, 2013), for a simply supported slab.

Finally, one-way shear resistance resulted to 513 kN for the closer load and to 572 kN for the further load.

For detailed calculations, see Appendix B4.

### 3.1.3 Flexural resistance

In addition to punching and one-way shear, the flexural resistance was calculated according to the yield line method.

Figure 19 shows a possible yield line pattern.

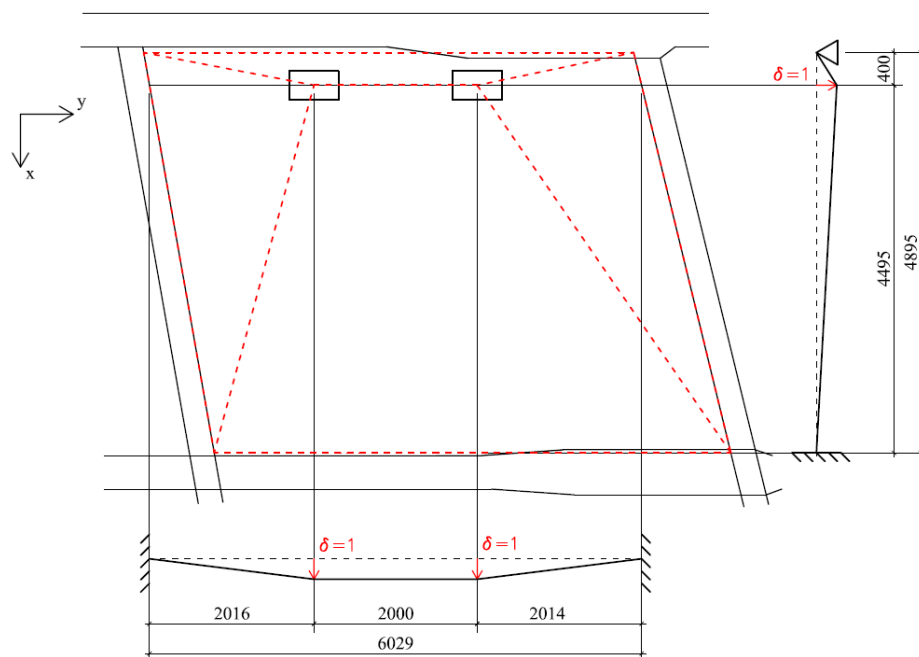


Figure 19: Yield line pattern for the bridge deck slab; all dimensions are in mm.

In accordance to determine the maximal loading capacity, the energy conservation principle was applied.

$$Q \cdot \delta = m_{Rd} \cdot L \cdot \theta \quad (15)$$

Where:

- $Q$  Applied load
- $\delta$  Vertical displacement due to applied load
- $m_{Rd}$  Moment resistance per meter of the yield line
- $L$  Length of yield line
- $\theta$  Rotation of the yield line

The bending resistance per meter was calculated as shown in equation (16).

$$m_{Rd} = a_s f_{sm} z = a_s f_{sm} \left( d - \frac{a_s f_{sm}}{2b f_{cm}} \right) \quad (16)$$

Finally, a load carrying capacity of 875 kN per loading plate resulted.

Detailed calculations concerning the reinforcement and the moment resistance can be found in Appendix B5.

### 3.1.4 Results and discussion

In Table 4 all results based on Level I analysis are summarized.

Table 4: Summary of results of Level I analysis.

Punching		One-way		Flexure	
Method	Capacity	Method	Capacity	Method	Capacity
EC	754 kN (CL)	EC	439 kN (CL)	Yield line	875 kN
	772 kN (FL)		477 kN (FL)		
MC	812 kN	MC	513 kN (CL)		
			572 kN (FL)		

\* CL = Closer loading point / FL = Further loading point

Based on above results, the slab would have collapsed due to one-way shear failure. To that it must be mentioned that for one-way shear calculations a simply supported slab was assumed. Since the top reinforcement layer continued over the support, actually, the slab was more than just simply supported. Thus, the calculated punching values from Table 4 may be raised.

It can be noticed that both Model code (CEB-FIP, 2013) and Eurocode 2 (EN 1992-1-1, 2004) delivered similar, yet conservative, values for punching and one-way shear.



## 3.2 Level II: Linear analyses

Numerical analyses became a more and more important tool for structural design and assessment of reinforced concrete structures. Thus, the usage of 3D finite element analyses has increased substantially in the last few years. Depending on the accuracy of the model linear or non-linear analyses can be performed. Linear analyses do not take either the non-linearity influence of the material into account nor the concrete cracking and reinforcement yielding.

In this study finite element software TNO Diana, Version 9.6 was used for computing and post-processing and Midas FX+, Version 3.1.0 for pre-processing.

### 3.2.1 Input parameters

#### 3.2.1.1 Element type

Depending on what type of results should be analysed the appropriate element type has to be chosen. Since the aim of this project was to evaluate the punching capacity for Level III assessment based on the critical shear crack theory, 2D curved shell elements were applied. These elements actually cannot describe out-of-plane shear, punching or anchorage failures (Plos et al., 2015). For Level II calculations local resistance models on higher levels of approximation according to Model code (CEB-FIP, 2013) were applied.

For each element in the mid-thickness of each layer four nodes were defined. Furthermore, in every element five degrees of freedom have been defined, this means three translations and two rotations.

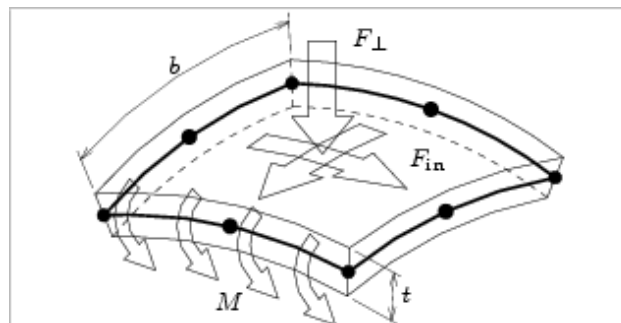


Figure 20: Curved shell element adopted from DIANA User's Manual (2014).

#### 3.2.1.2 Material models

For linear analyses a linear relationship between stress and strain is assumed. Therefore, isotropic models for steel and concrete were applied. Thus, the material properties that were used for linear analyses are Young modulus of concrete, Poisson's ratio as well as mass density of concrete. The material parameters which were used for FE performance are listed in Table 1.

#### 3.2.1.3 Boundary conditions

For linear FE analyses the boundary conditions as shown in Figure 12 were applied. This means simply supported at the outside girder and fully fixed along the other three borders.

#### 3.2.1.4 Mesh density

In finite element analyses mesh size is a crucial factor since the quality of a model depends on it. Thus, FE models with fine mesh (small element size) yields highly accurate results but may take longer computing time as well as more efforts for meshing are required. On the other hand, FE calculations with coarse mesh (large element size) may lead to less accurate results but smaller computing time.

The present bridge deck slab was meshed with quadrilateral curved shell elements of size 50 mm x 50 mm. This high mesh density was chosen in order to model the loading area which was close to the side girder as precisely as possible.

#### 3.2.1.5 Integration schemes

For describing the slab, in plane a 2x2 Gauss integration scheme was used. In the thickness direction, for linear FE analyses the software automatically divides the slab into three layers.

### 3.2.2 FE-Modelling

The slab was modelled as shown in Figure 21 and Figure 22. Thereby, the slab part with varying thickness was modelled as segments, with each segment having its own thickness.

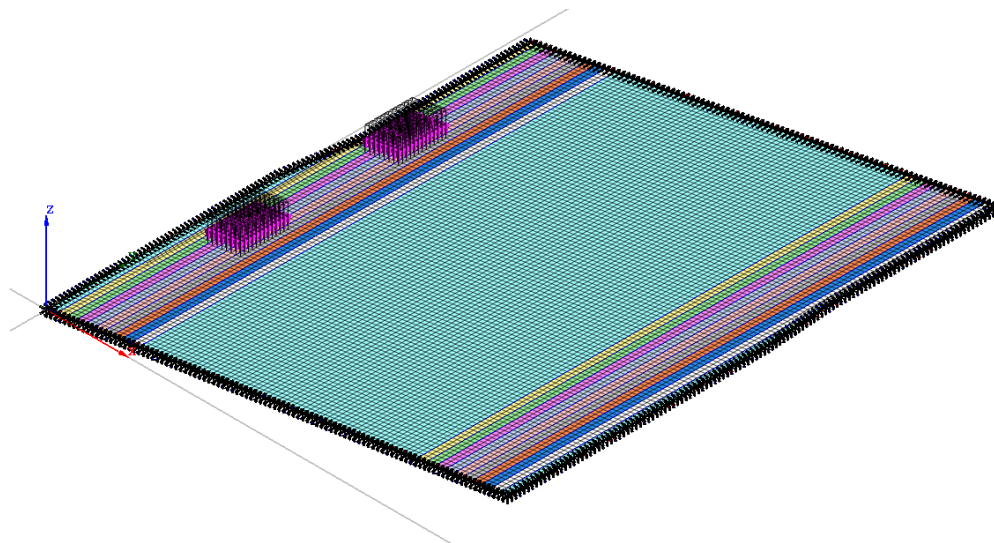


Figure 21: FE Model including loading points and boundary conditions.

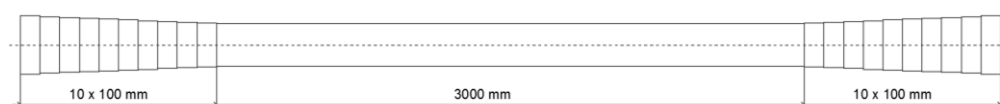


Figure 22: Cross section of the shell elements showing segments with varying thickness.

### 3.2.3 Punching shear resistance

#### 3.2.3.1 Eurocode 2

According to Eurocode 2 (EN 1992-1-1, 2004) there exists no advanced approximation in order to calculate the punching shear resistance. Thus, the resistance remained the same as for Level I assessment.

#### 3.2.3.2 Model code

In Model code (CEB-FIP, 2013), as mentioned in Chapter 2.2.1, several levels of accuracy may be applied, since the control perimeter  $b$  as well as the rotation perimeter  $\psi$  can be refined.

The rotation factor is calculated at level II approximation as listed in equation (17).

$$\psi_{II} = 1.5 \frac{r_s}{d} \frac{f_{yd}}{E_s} \left( \frac{m_{Ed}}{m_{Rd}} \right)^{1.5} \quad (17)$$

According to Model code (CEB-FIP, 2013) the average bending moment acting in the support strip ( $m_{Ed}$ ) can be approximated for each reinforcement direction and support type. Since the load can be transported in all four directions, an inner column was assumed. Based on this assumption the average bending resistance may be determined according to equation (18). The flexural strength per unit length in the support strip was calculated as shown in equation (19).

$$m_{Ed} = V_{Ed} \cdot \left( \frac{1}{8} + \frac{|e_{u,i}|}{b_s} \right) \quad (18)$$

$$m_{Rd} = a_s f_{sm} z = a_s f_{sm} \left( d - \frac{a_s f_{sm}}{2b f_{cm}} \right) \quad (19)$$

For simplified calculations, the factor refers to the eccentricity was not taken into account. Consequently, the average bending moment per unit length was assumed to be  $m_{Ed} = V_d/8$ . Since  $V_{Ed}$  in equation (18) represents the load which is added before punching failure occurs, it will be an iterative approach to provide the rotation factor  $\psi_{II}$ . For the first approximation the calculated load  $V_{Ed} = 812$  kN from Level I analysis was used.

Additionally, level III approximation for the rotation factor exists, which are recommended especially for irregular slabs or for slabs where the ratio of span lengths  $L_x/L_y$  is not between 0.5 and 2.0. According to Model code (CEB-FIP, 2013) the approximation may be used preferably for uncracked linear elastic model.

$$\psi_{III} = 1.2 \frac{r_s}{d} \frac{f_{yd}}{E_s} \left( \frac{m_{Ed}}{m_{Rd}} \right)^{1.5} \quad (20)$$

### Results gained with the basic control perimeter $b_1$

By using rotation factor  $\psi_{II}$  the punching capacity followed to 233 kN. For rotation factor approximation level III ( $\psi_{III}$ ) a punching capacity of 286 kN resulted.

Detailed calculations based on  $b_1$  can be found in Appendix C1.

### Results gained with the shear-resisting control perimeter $b_0$

Instead of calculating with the basic control perimeter  $b_1$ , the shear-resisting control perimeter  $b_0$  can be used.

The punching shear resistance is calculated similarly to equation (6).

$$V_{Rd,c} = v_{Rd,c} b_0 d \quad (21)$$

The shear-resisting control perimeter  $b_0$  is determined according to Model code (CEB-FIP, 2013) as shown in equation (22).

$$b_0 = \frac{V_{Ed}}{V_{perp,d,max}} \quad (22)$$

Thereby  $V_{Ed}$  expresses the design shear force value and  $V_{perp,d,max}$  the maximal shear force per unit length perpendicular to the basic control perimeter.

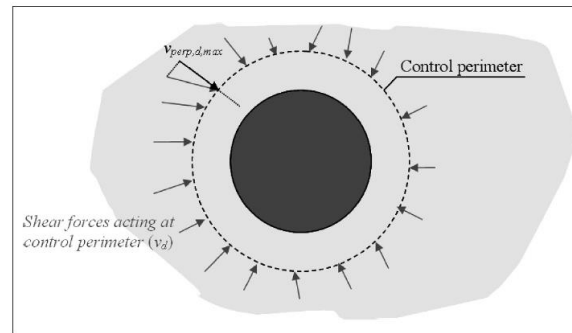


Figure 23: Shear force per unit length ( $v_d$ ) and maximum value perpendicular to the basic control perimeter according to Model code (CEB-FIP, 2013).

For determining the maximal shear force along the control perimeter, the shear distribution was extracted out of the linear FE model, see Figure 24. Besides, the irregularities along the support can be neglected since they do not affect the result.

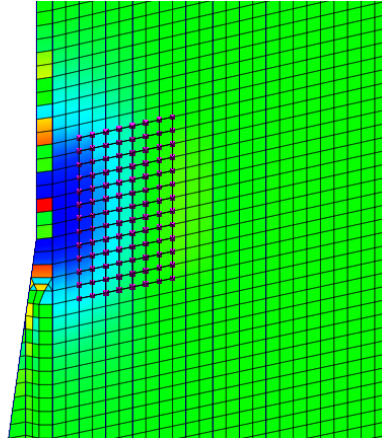


Figure 24: Shear distribution  $q_{yz}$  around loading point (closer load).

Since the loading plate was located very close to the support, the shear distribution was very unsymmetrical. This came, since the applied load was absorbed mainly from the closest support. Hence an unusual high value for the maximal shear force per unit length perpendicular to the basic control perimeter resulted. On the other hand, the shear value along the control perimeter in the middle of the plate became an even negative value.

Figure 25 shows the shear distribution along the control perimeter with a maximal shear force of  $V_{perp,d,max} = 414$  kN due to an added load of  $V_{Ed} = 500$  kN. Finally, the shear-resisting control perimeter  $b_0$  followed to 1.21 m.

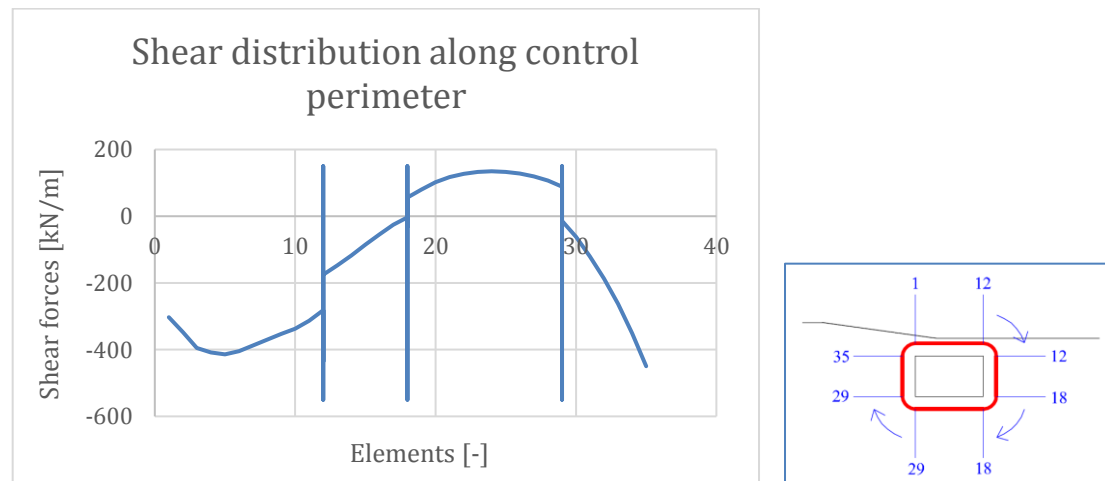


Figure 25: Shear distribution along control perimeter.

Even though the shear-resisting control perimeter was unrealistically low, calculations had been done according to Model code (CEB-FIP, 2013). Finally, punching capacities of 377 kN, 108 kN and 133 kN resulted for approximation levels  $\psi_I$  to  $\psi_{III}$ .

Detailed calculations can be found in Appendix C2.

### 3.2.4 One-way shear resistance

For Level II assessment the effective width was calculated with a more advanced method based on a Swedish recommendation for finite element analysis (Pacoste et al., 2012). The method is explained and simultaneously applied in the current chapter.

#### Location of critical section and effective width according to the Swedish recommendation (Pacoste et al., 2012)

In a first step the distribution width was calculated according to the Swedish recommendation (Pacoste et al., 2012). It states that for a group of forces situated in the same row, the critical cross section for shear forces is always placed at a distance  $y_{cs} = (c + d)/2$  from the center of the loading points.

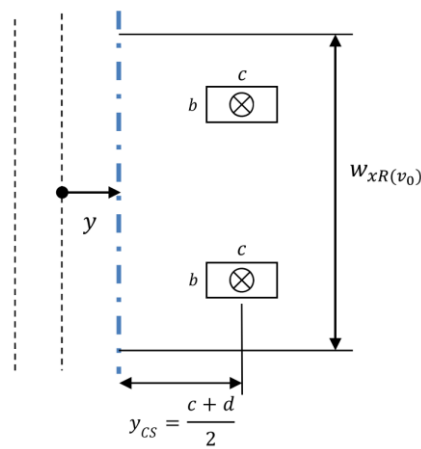


Figure 26: Location of the critical cross section and width of the section as recommended in the Swedish recommendation (Pacoste et al., 2012).

In order to get the effective depth at the critical section  $d$  as well as the location of this section, which depends on the effective depth, two equations had to be combined. Thus, the effective depth was determined by solving the following system of equations for  $d$ . The length of the loading point was  $c = 350$  mm.

$$d = 223 + \frac{246 - 223}{330} \cdot \left( \frac{c + d}{2} \right) \quad (23)$$

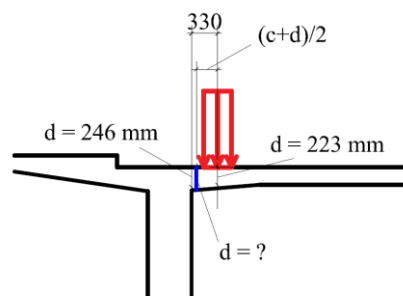


Figure 27: Approach to determine the effective depth at the critical cross section.

It resulted an effective depth of 244 mm at the critical cross section in a distance of  $(c + d)/2 = 297$  mm from the center of the load.

In conclusion, the width of the critical section is calculated as the minimum of two terms, see equation (24).

$$w = \min(7d + b + t; 10d + 1.3y_{cs}) \quad (24)$$

Where  $b$  expresses the width of the loading area and  $t$  the thickness of the surfacing, which was assumed to be zero. Finally, for the cross section a width of 2.31 m resulted for one loading point. Since the widths of the loading plates overlapped in the middle, in total a width of 4.31 m resulted in a distance of 297 mm from the center of the load.

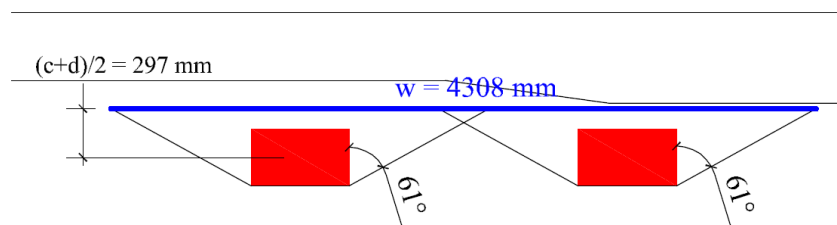


Figure 28: Location of the critical section and effective width.

### Calculating one-way shear resistance by using linear material behaviour of Level II assessment

In the further course, linear material behaviour was used to determine the one-way shear resistance. Since in Level II assessment the load-shear relationship is linear, see Figure 29, a random load could be applied in the FE modelling in order to get the corresponding average shear value along the critical section. Including the calculated shear force from Level I assessment, the one-way shear resistance from Level II analysis could be determined.

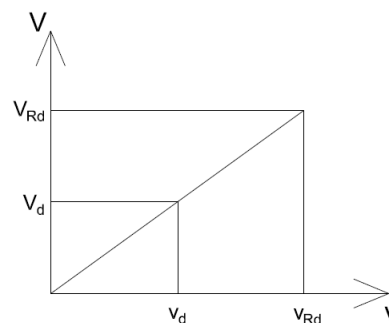


Figure 29: Linear relationship between capacity and shear resistance.

$$\frac{V_d}{v_d} = \frac{V_{Rd}}{v_{Rd}} \rightarrow V_{Rd} = \frac{V_d}{v_d} v_{Rd} \quad (25)$$

Where:

- $V_{Rd}$  Maximal one-way shear resistance
- $V_d$  Random load applied at FE modelling
- $v_d$  Average value of the shear forces along the width due to  $V_d$
- $v_{Rd}$  Average shear force resistance from Level I calculation

With an added load of  $V_d = 500$  kN per loading plate, an average shear force resistance along the critical width of  $v_d = 168$  kN/m resulted. Figure 30 shows the shear distribution along the critical section (blue line) and the average shear resistance along the critical width of 4.31 m (red line). The maximal peak came from the load which was placed closer to the support.

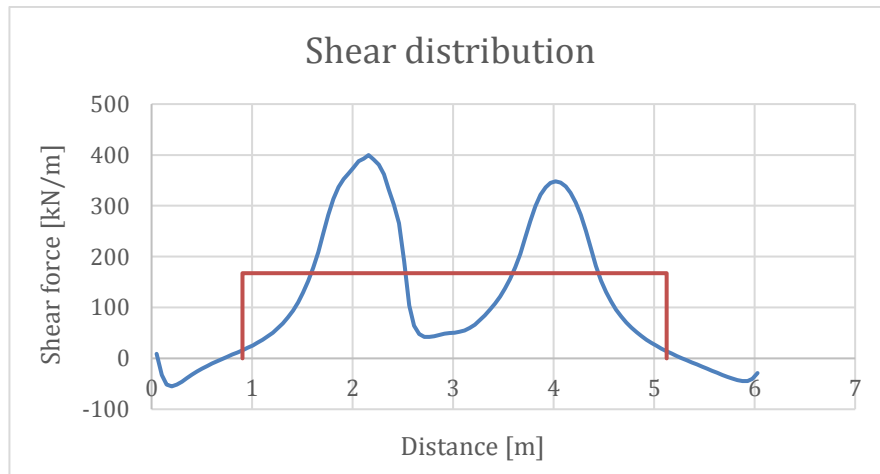


Figure 30: Shear force distribution along critical cross section (blue line) and distribution width with average shear force value (red line).

The average shear force resistance based on Model code (CEB-FIP, 2013) in Level I assessment followed to  $513 \text{ kN} / 2.080 \text{ m} = 247 \text{ kN/m}$  and consequently a one-way shear resistance of  $V_{Rd} = 735 \text{ kN}$  resulted for Level II assessment.



### 3.2.5 Flexural resistance

For Level II flexure assessment also the Swedish recommendation (Pacoste et al., 2012) was used. The distribution width for moments is identical to the distribution width for shear forces (Chapter 3.2.4) and accounted for 4.31 m.

The linear behaviour of Level II assessment was used in order to get the maximal flexural resistance.

$$\frac{V_d}{m_d} = \frac{V_{Rd}}{m_{Rd}} \rightarrow V_{Rd} = \frac{V_d}{m_d} m_{Rd} \quad (26)$$

Where:

- $V_{Rd}$  Maximal one-way shear resistance
- $V_d$  Random load applied at FE modelling
- $m_d$  Average value of bending forces along the width due to  $V_d$
- $m_{Rd}$  Average flexure resistance from Level I calculation

Along the critical section an average flexural resistance of  $m_d = 20.2$  kNm resulted due to a load of  $V_d = 500$  kN per loading plate. The maximal peak represents the load which was placed further to the support.



Figure 31: Moment distribution along critical cross section (blue line) and distribution width with average bending value (red line).

The resistance of the top reinforcement layer along the section was calculated to  $m_{Rd} = 37.7$  kNm (Appendix B5).

The flexural resistance followed to  $V_{Rd} = 933$  kN.

### 3.2.6 Results and discussion

The results from Level II assessment are summarized in Table 5.

Table 5: Summary of results of Level II analysis.

Punching		One-way		Flexure	
Method	Capacity	Method	Capacity	Method	Capacity
MC ( $b_1$ )	233 kN ( $\psi_{II}$ )	Linearity properties	735 kN	Linearity properties	933 kN
	286 kN ( $\psi_{III}$ )				
MC ( $b_0$ )	377 kN ( $\psi_I$ )				
	108 kN ( $\psi_{II}$ )				
	133 kN ( $\psi_{III}$ )				

By considering the punching results, it is obvious that all values are very conservative. In order to explain these low values, there are two main reasons which have to be mentioned. First of all, by comparing the results gained with rotation perimeter  $\psi_I$ , with results provided with rotation perimeter  $\psi_{II}$  or  $\psi_{III}$ , the differences are distinctive. The reason for this must lay in the bending moment redistribution which is considered additionally for  $\psi_{II}$  and  $\psi_{III}$ , see equations (17) and (20). Thereby, either the average moment per unit length  $m_{Ed}$  was calculated to optimistic or else the average flexural strength per unit length  $m_{Rd}$  was assumed to be underestimated. Since for the impact already a low value  $V_{Ed} = 812$  kN from Level I assessment was applied, the problem must come from the considered bending resistance of the slab. The main reason for this was found in the arrangement of the reinforcement, see also Figure 4. Since the loading areas were placed very close to the support, the main reinforcement layer was located at the top of the slab. On the other hand, the bottom reinforcement layer comprised only  $\emptyset 10@270$  ( $m_{Rd} = 37.7$  kN) in x-direction and  $\emptyset 10@250$  ( $m_{Rd} = 46.4$  kN) in y-direction, which corresponded to the minimum reinforcement. For the even lower values gained with the shear-resisting control perimeter  $b_0$ , the one-way shear distribution, as shown in Figure 24, was responsible. Hence a calculated shear-resisting control perimeter  $b_0 = 1208$  mm was less than half of the basic control perimeter  $b_1 = 2601$  mm.

One-way shear resistance was calculated by using linear material behaviour. Thereby, the maximal shear force according to Level I assessment and the shear distribution, which was extracted along the effective width  $w$ , was considered. Compared to Level I assessment a higher, yet conservative, value was evaluated.

For calculating the flexural resistance also the linear behaviour was taken into account. Finally a similar result was occurred as in Level I analysis.

### 3.3 Level III: Non-linear analyses

In contrast to linear analyses, for non-linear assessments the loads are applied gradually on the model until failure of the structure is reached. Thus, non-linear analyses are the perfect tool to get more realistic results. According to Broo *et al.* (2008) there are two main reasons for the higher capacities evaluated with non-linear finite element programs. First, by analysing in three dimensions the load distribution is more appropriate and second, in numerical analyses the fracture energy due to concrete cracking is also included. However, it is important to have a good understanding of all input parameters since this is the basis to achieve most accurate results.

#### 3.3.1 Input parameters

##### 3.3.1.1 Element type

As used for linear analyses also for non-linear assessments 2D curved shell elements (Figure 20) were applied. Since shell elements do not describe out-of-plane shear or punching, these failure modes have to be checked by the critical shear crack theory of Muttoni (Chapter 2.3).

##### 3.3.1.2 Concrete

To describe non-linear behaviour of concrete in a realistic way stress-strain curves according to Hordijk for tension and Thorenfeldt for compression were used. Since both approaches are based on total strains and the concrete cracking, the strategy is called total strain crack theory.

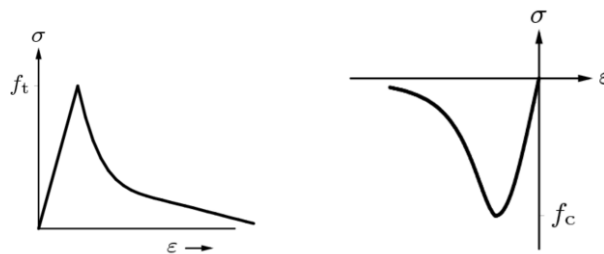


Figure 32: Material models for concrete: Hordijk in tension (left) and Thorenfeldt in compression (right), adopted from DIANA User's Manual (2014).

The crack distance was calculated to be 219 mm based on Eurocode 2 (EN 1992-1-1, 2004). Detailed calculations can be found in Appendix E1. Thereby, the rotating crack model was used. This means according to DIANA User's Manual (2014) that the crack direction is always perpendicular to the principal stress direction and no shear crack along the crack occurs. The fracture energy was determined to be 154 N/m according to Model code (CEB-FIP, 2013), see also Appendix E2. The cracking model used in the FE modelling is called smeared crack approach. It was assumed that a new crack is smeared over a region. The length of this cracked region is called crack band width (Hakimi, 2012).

### 3.3.1.3 Reinforcement

According to the multi-level assessment strategy, for Level III assessment it is assumed that the reinforcement is fully embedded in the concrete, i.e. it has perfect bond to the concrete. According to Plos *et al.* (2015) for modelling embedded reinforcement, plane shaped reinforcement grids are the preferably tool. Thus, for both directions the volume of the reinforcement layer was determined to be equal to the volume of the reinforcement bars. The level of the reinforcement layers was determined under assumption that the effective depth issued from  $d = 0.85 t$ , see Figure 33.

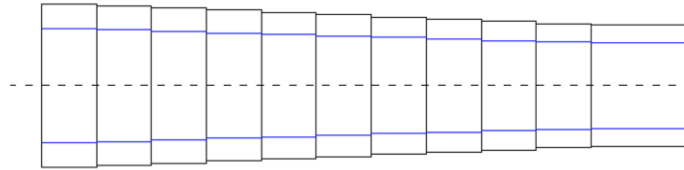


Figure 33: Level of reinforcement layers in elements with varied thickness.

### 3.3.1.4 Boundary conditions

In order to get appropriate results it was important to choose right boundary conditions. In many case studies it is difficult to find the right boundary conditions since in reality often an intermediate rigidity between fully fixed and simply supported may be appropriate.

### 3.3.1.5 Mesh density

The present bridge deck slab was meshed with mainly quadrilateral curved shell elements of size 50mm x 50mm. This high mesh density was chosen in order to model the loading area, which is close to the side girder, as precisely as possible.

### 3.3.1.6 Interpolation function and integration schemes

Since geometry of the investigated slab was not very ordinary, for the mesh scheme quadrangular and triangular elements were needed. Thus, in the plane a 2x2 Gauss integration scheme was used for quadrilateral elements and a three point Gauss integration scheme for triangular elements. Over the height of the elements, i.e. in the thickness direction a nine point Simpson integration scheme was applied.

### 3.3.1.7 Iteration method & convergence criteria

With the iteration method the computing time can be limited (Broo *et al.*, 2008). For all analyses, Newton-Raphson iteration method with a tangential convergence criteria of 0.01 was used. According to DIANA User's Manual (2014) the regular Newton-Raphson iteration is based on the tangential stiffness of the structure and provides a final result within only a few iterations. For the convergence criteria, the energy norm ratio was used. According to DIANA User's Manual (2014) this criteria bases on the internal energy, which is expressed as the area under the load-displacement curve.

### 3.3.2 FE Analysis

#### 3.3.2.1 Load method

As mentioned in the introduction, the main difference of a non-linear analysis compared to a linear analysis is that loads are applied gradually on the model. As showed in a previous master's thesis (Hakimi, 2012), the load stepping process can be done with three different methods, called load-controlled, displacement-controlled and arc-length incrementation. In the following master's thesis the load- and displacement-controlled methods were applied.

#### Load-controlled method

In the load-controlled method, while increasing the load, the program searches for a displacement field that corresponds to the applied load (Hakimi, 2012).

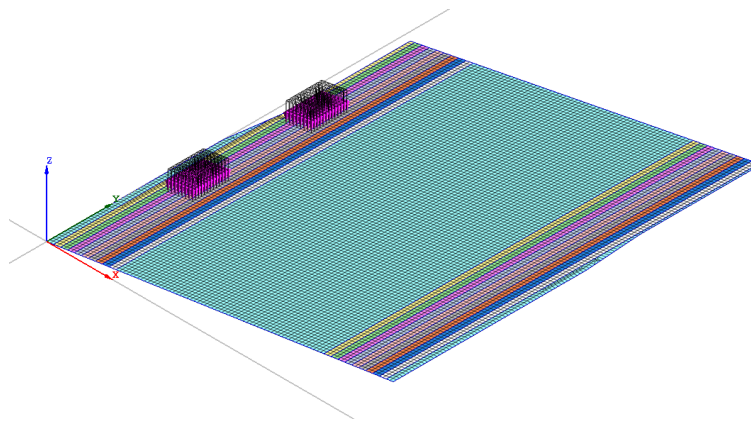


Figure 34: FE model showing loads which are added based on the load-controlled method.

#### Displacement-controlled method

In contrast to applying load forces, in the displacement-controlled method increasingly displacement is added. Due to displacement of a set of nodes, the equilibrium is found by searching for the corresponding forces.

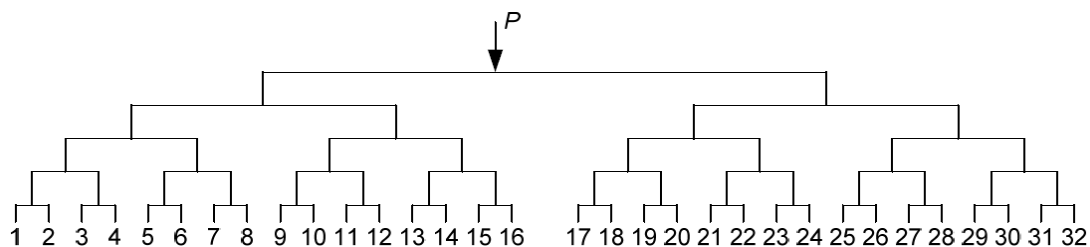


Figure 35: Applying the vertical load in total 32 points (16 per loading area) on the slab, using statically determined arrangement of stiff beams. Illustration adopted from Broo et al. (2008).

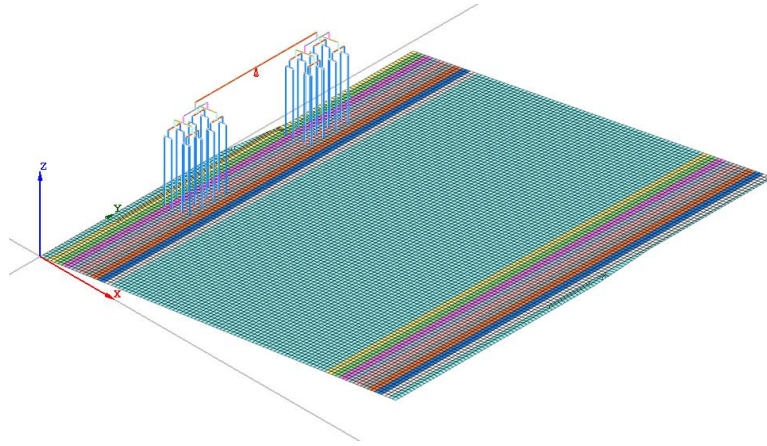


Figure 36: FE model showing loads which are added based on the displacement-controlled method.

As a condition in order to get rational results, for horizontal beams the bending stiffness and for vertical links the axial stiffness were determined to be infinite. The selected degrees of freedom for the horizontal connections can be viewed in Figure 37. Further, it was important that the displacement force was added in the middle of the horizontal beams because only in this way the displacement was transferred correctly to the bottom links.

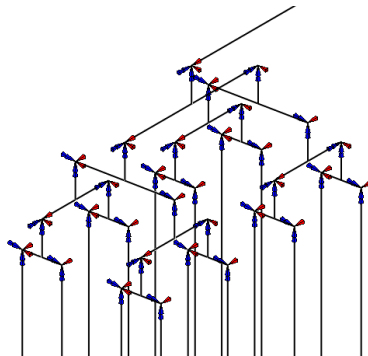


Figure 37: Detailed part of the displacement model including boundary conditions (red = translation, blue = rotation).

### 3.3.2.2 Results of analyses and comparison to the experiment

In order to assess the suitability of the FE model the load-rotation curve was analysed and compared with test measurements, see Figure 38. In this way the stiffness of the model could be evaluated.

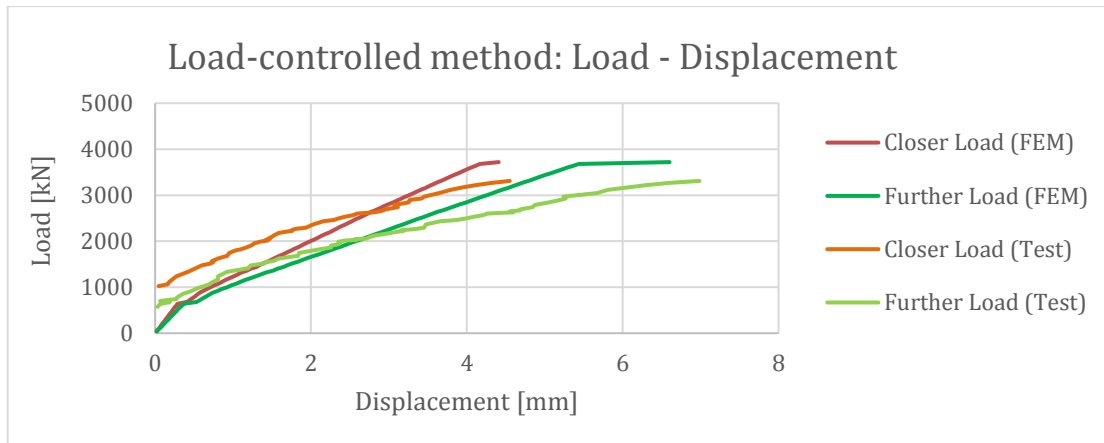


Figure 38: Load-displacement curves for a simply supported slab.

By analysing Figure 38, it can be stated that the curves from the non-linear FE analysis increase faster. This means that the stiffness of the FE model is minimally stiffer compared to the reality. However this small difference may also have other reasons, such as measurement inaccuracies. In conclusion it can be summarized that the chosen material properties as well as the assumption of a simply supported slab describe the real behaviour of the slab very accurate.

Furthermore, to ensure that cracks happened in the right place, the strain based crack pattern was examined, see Figure 39.

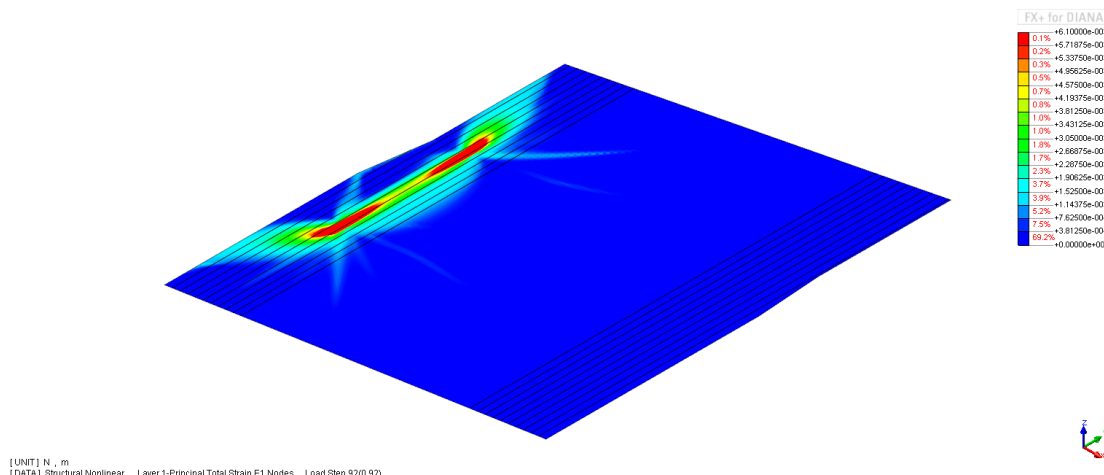


Figure 39: Strain based crack pattern before failure occurred.

The red marked regions show where the reinforcement started yielding. The initial yield stress was set to 610 MPa in the non-linear FE analysis.

Since shell elements cannot describe punching shear failure, only the in-plane crack pattern depending on the bending moments can be outputted. Thus it must be mentioned, that the showed crack pattern does not represent the reality accurate. However, the locations and also the pattern of the reinforcement yielding were plotted correctly.

### 3.3.3 Punching shear resistance

For Level III assessment, the critical shear crack theory by Muttoni was applied. As explained in Chapter 2.3, the total punching capacity results at the intersection of the failure curve and the load-rotation curve (point A in Figure 40).

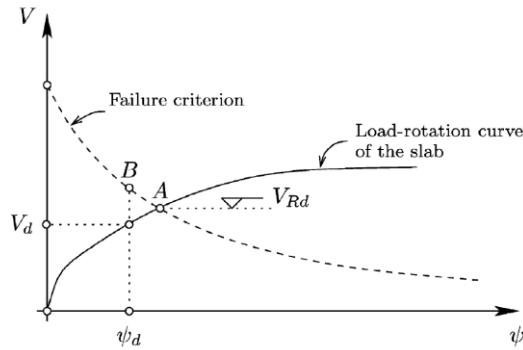


Figure 40: Approach to determine the punching capacity based on the CSCT.

Table 6: Input parameters for calculating the punching capacity according to the CSCT.

Input parameters for CSCT	
Load-controlled	$V = 0, 40, 80, 120, 160, \dots$ [kN]
Displacement-controlled	$d = 0.1, 0.2, 0.3, 0.4, 0.5, \dots$ [mm] $\rightarrow V = \dots$
Muttoni: Failure criterion	$\psi_{Failure} = \left( \frac{3/4 b d \sqrt{f_{cm}}}{V} - 1 \right) \frac{d_{g0} + d_g}{15 d}$
FEM: Load-rotation curve	$\psi_{Load-Rot.} = \frac{Displacement (V)}{Length}$

Since in the current case study the two loading plates were not placed in the same distance from the support, the displacement below the plates was not equal. Consequently, two load-rotation curves had to be determined.

The parameters which were applied for the CSCT are summarised in Table 7.

Table 7: Basic perimeters which were used for the CSCT.

Basic perimeters		
Control perimeter	$b$	2601 mm
Effective depth	$d$	223 mm
Average concrete compressive strength	$f_{cm}$	62.2 MPa
Reference size equal to 16 mm	$d_{g0}$	16 mm
Maximum size of the aggregate	$d_g$	16 mm



In order to get the values of rotation  $\psi$ , for both loading plates the difference in rotation at point  $P_1$  and  $P_2$  was calculated.

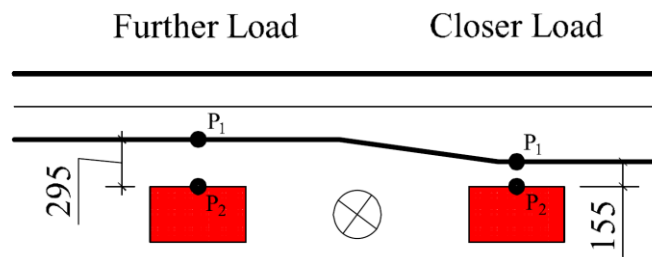


Figure 41: Approach to determine the rotation angle of the slab  $\psi$ .

After performing the non-linear analysis, the load-rotation curves could be drawn as shown in Figure 42 based on the load-controlled method and in Figure 43 based on the displacement-controlled method.

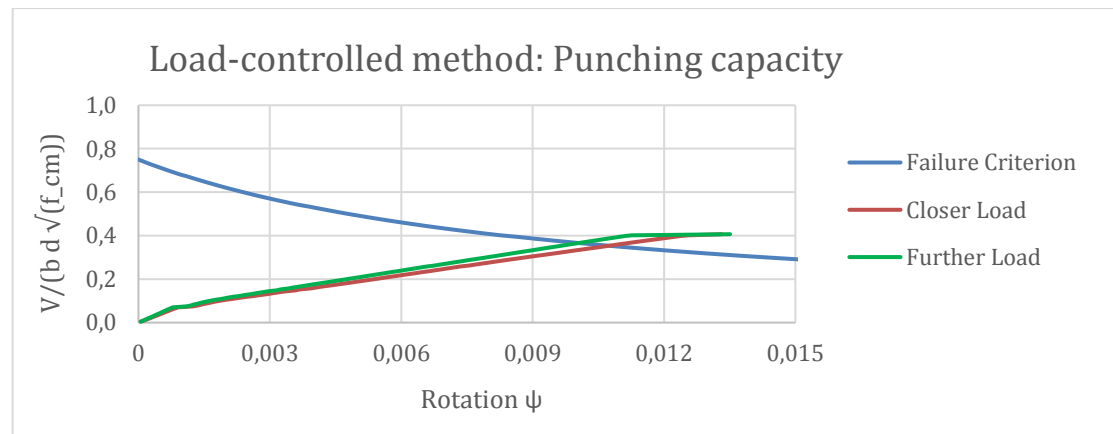


Figure 42: Punching capacity calculated based on the load-controlled method for simply supported slab.

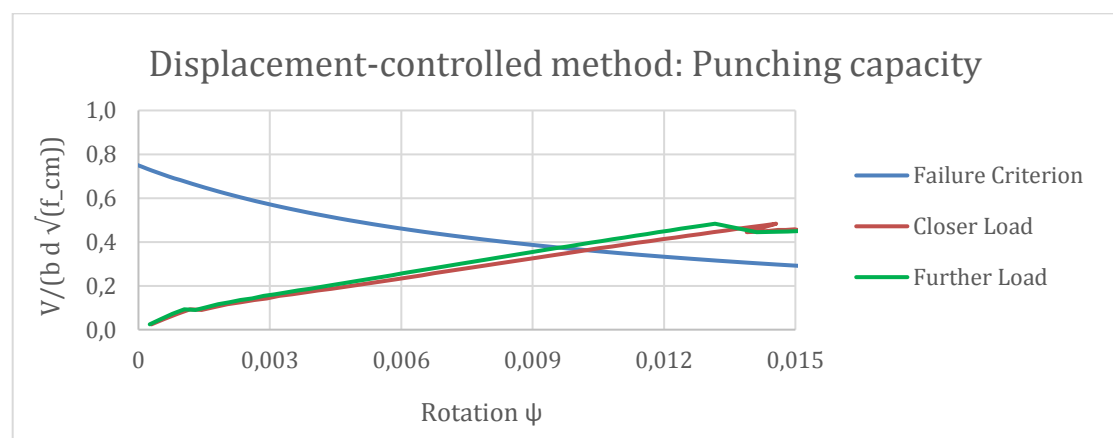


Figure 43: Punching capacity calculated based on the displacement-controlled method for simply supported slab.

At the cross sections of the two curves a punching capacity of 1617 kN for the closer load and a capacity of 1672 kN for the further load resulted due to the load-controlled method.

Analyses based on the displacement-controlled method delivered punching capacities of 1658 kN and 1711 kN for the closer and the further load, respectively.

### 3.3.4 One-way shear resistance

For Level III one-way shear calculation there exists no known method which yields more accurate results than Level II analysis.

### 3.3.5 Flexural resistance

The flexural resistance was determined by analysing the load-displacement relationship. Since shell elements are not designed to describe shear failure, non-linear FE analyses interrupt when the flexural resistance is reached. Figure 44 and Figure 45 show the load-displacement curves as well as the measured test results.

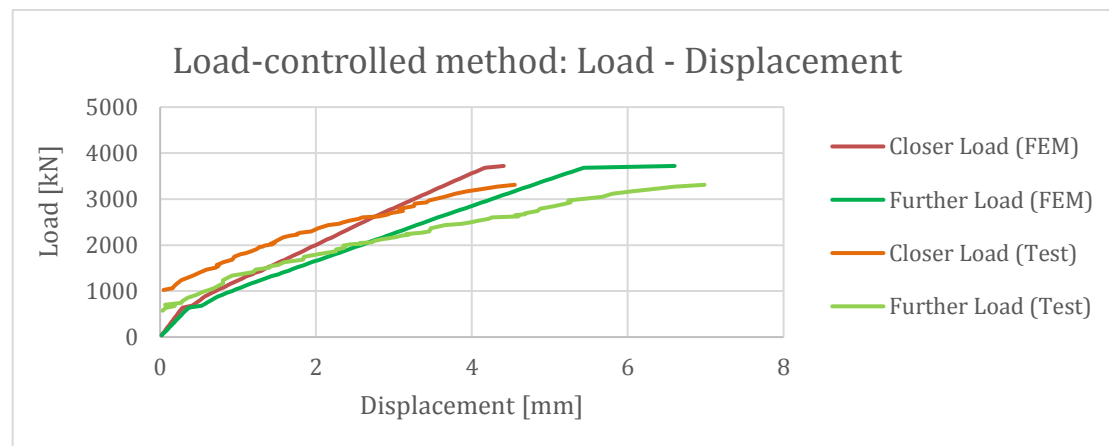


Figure 44: Load-displacement curves for simply supported slab based on the load-controlled method.

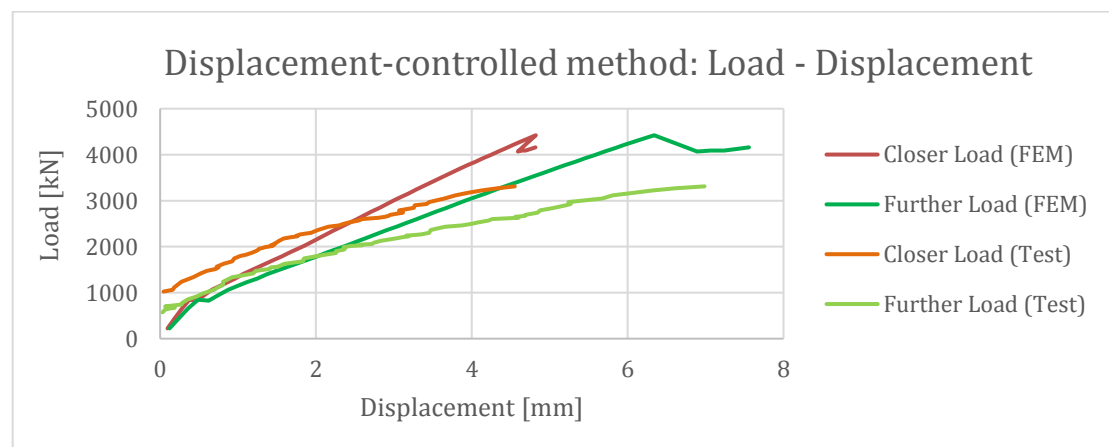


Figure 45: Load-displacement curves for simply supported slab based on the displacement-controlled method.

The flexural resistance followed to 3720 kN based on the load-controlled method and to 4420 kN based on the displacement-controlled method. These loads represented the total applied load, which means the load for both loading plates.

### 3.3.6 Results & discussion

Table 8 shows the results from Level III assessment.

Table 8: Summary of results of Level III analysis by assuming a simply supported slab.

Punching		One-way		Flexure	
Method	Capacity	Method	Capacity	Method	Capacity
CSCT (LM)	1617 kN (CL)	-	-	Non-lin. FE (LM)	1860 kN
	1672 kN (FL)				
CSCT (DM)	1658 kN (CL)			Non-lin. FE (DM)	2210 kN
	1711 kN (FL)				

\* CL = Closer loading point / FL = Further loading point

LM = Load-controlled method / DM = Displacement-controlled method

It can be stated that for both loading points the punching capacity was similar to test results, where failure occurred by an added load of 1660 kN. The difference between the two applied load methods was minimal according to the punching capacity, but bigger regarding the flexural resistance.

Furthermore, it can be stated that the critical shear crack model represented the punching capacity correctly, also if loads were placed close to the support.

### 3.4 Results and discussion

In this chapter all results gained according to the multi-level assessment strategy are summarised and discussed.

#### 3.4.1 Punching shear resistance

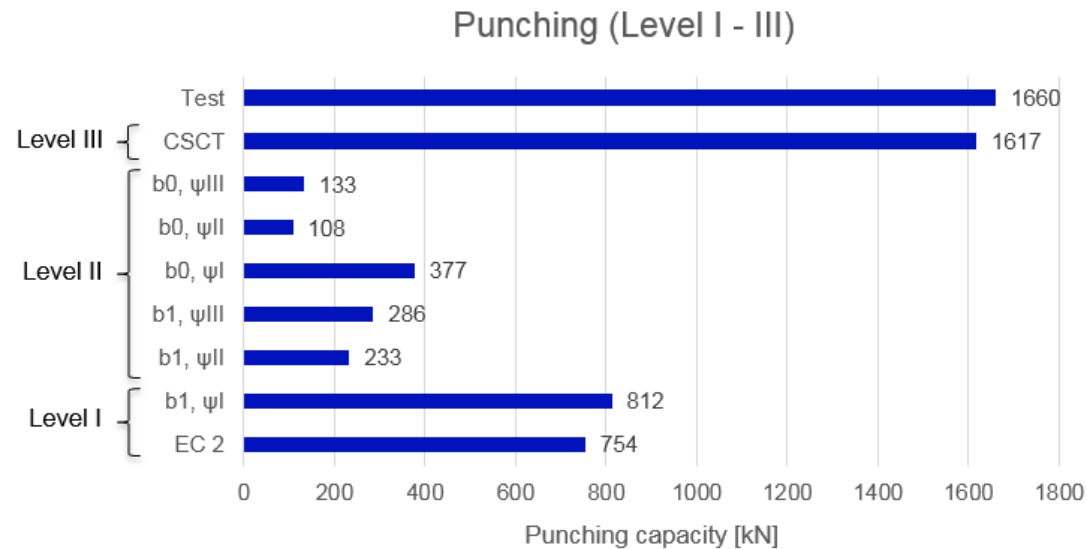


Figure 46: Summary for punching capacities for Level I – III.

The punching results for Level I and III assessments were as expected. On the other hand, for Level II assessment the results gained with an advanced rotation perimeter  $\psi$  and with the shear-resisting perimeter  $b_o$  did not lead to accurate results.

As shown in Chapter 3.2.3.2, by replacing the basic control perimeter  $b_1$  with the shear-resisting perimeter  $b_o$ , the results became even worse. The reason was found in the unsymmetrical shear distribution around the loading area. Since the loading plates were located close to the support, the shear distribution resulted very unsymmetrical, see Figure 24. Thus the load was transported mainly in one-way, i.e. to the closer support. Hence an unusual high value for the maximal shear force per unit length perpendicular to the basic control perimeter resulted and consequently an unrealistic low value for the shear-resisting perimeter.

Responsible for the lower values obtained with an advanced rotation perimeter  $\psi$ , was the low reinforcement ratio below the loading plates. Thus a low bending resistance for the slab resulted and consequently a minimal load carrying capacity.

### 3.4.2 One-way shear resistance

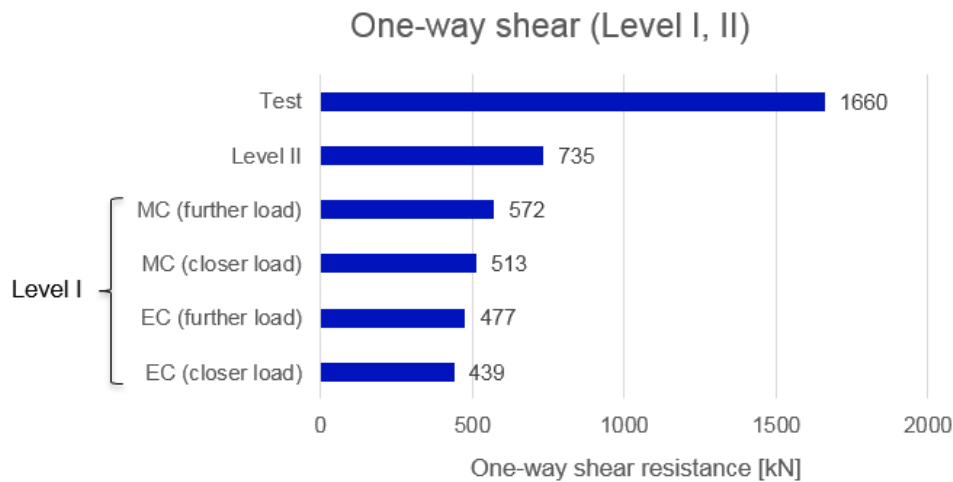


Figure 47: Summary for one-way shear capacities for Level I & II.

Considering Level I results, it can be stated that Eurocode 2 (EN 1992-1-1, 2004) delivered more conservative results compared to Model code (CEB-FIP, 2013). Furthermore, it can be concluded that the closer a load was placed to the support, the smaller one-way shear resistance came to. This is logical since the critical width became smaller and as a result the shear force could not be smeared over a wide length.

For Level II one-way shear assessment an improved validation was achieved in comparison to Level I assessment. Thus it can be summarized that the application of the Swedish recommendation (Pacoste et al., 2012) was useful to obtain the location of the critical section as well as the width of it. In addition with the gained one-way shear resistance from Level I and also based on the linear material behaviour of Level II assessment, an advanced validation of the one-way shear capacity could be achieved.

### 3.4.3 Flexural resistance

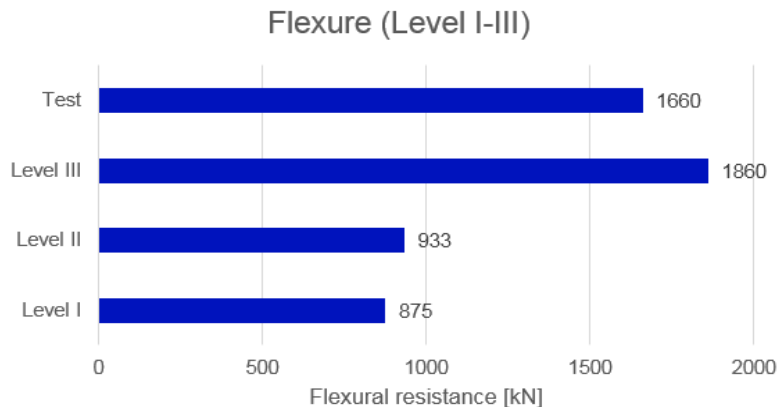


Figure 48: Summary for flexure capacities for Level I – III.

The flexure assessment showed a successively improved evaluation in structural assessment.

The application of the yield line method in Level I delivered a conservative value, since it was assumed that the slab was simply supported. In reality for bending along the outside girder, energy will be transformed according to the applied energy conservation principle. Thus the underestimation for the flexural resistance would not be as immense.

Level II flexure assessment, based on linear material behaviour and on the average moment distribution along the critical section, delivered advanced results, compared to Level I analysis. However, the results were very conservative. Thus the application of the Swedish recommendation (Pacoste et al., 2012) has to be considered carefully. Since the critical section was determined to be next to the support, see Figure 28, the moment distribution got minimal values for a simply supported slab.

Level III assessment delivered an overestimated value compared to the test results. However, since flexure was not expected to be the decisive failure mode, this value was reasonable.

## 4 Parameter Study

In the following chapter the influence of certain parameters was analysed. Thereby a main focus lied on the influence of boundary conditions on the result. In order to assess this influence, in Chapter 4.1 all calculations according to the multi-level assessment strategy had been performed again. In contrast to the previous chapters, a fully fixed slab was assumed.

In a second parameter study in Chapter 4.2 the influence of the effective depth on the punching capacity was analysed. Thereby only Level III punching assessment according to the critical shear crack theory was performed.

### 4.1 Influence of boundary conditions

In this chapter, in contrast to the previous part of this thesis, it was assumed that the slab was fully fixed at the outside girder, see Figure 49.

The parameters used for calculations in this chapter are listed in Table 7.

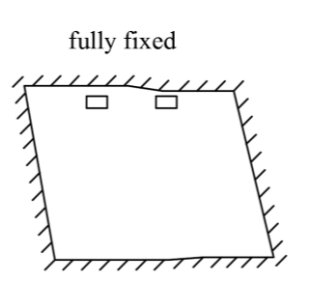


Figure 49: Fully fixed slab along all borders.

#### 4.1.1 Level I

##### 4.1.1.1 Punching resistance

Neither in Model code (CEB-FIP, 2013) nor in Eurocode 2 (EN 1992-1-1, 2004) the boundary conditions are considered regarding the punching capacity. Thus the results were equal to the values gained by assuming a simply supported slab.

##### 4.1.1.2 One-way shear resistance

If assuming a clamped slab the load distribution angle should be taken as  $\alpha = 45^\circ$  according to Model code (CEB-FIP, 2013).

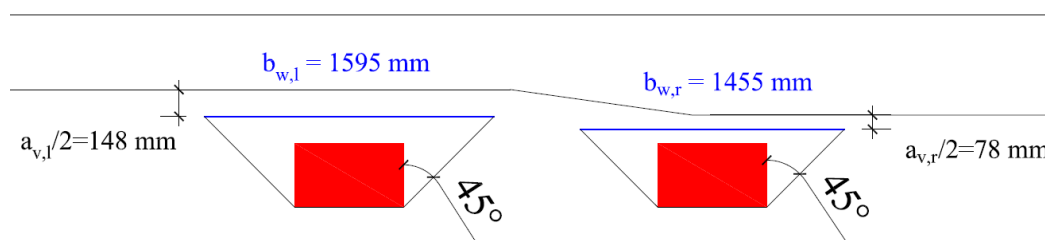


Figure 50: Critical width according to Model code (CEB-FIP, 2013) for a clamped slab.

Furthermore, if assuming a fully anchored reinforcement at the support, in both Model code (CEB-FIP, 2013) and Eurocode 2 (EN 1992-1-1, 2004), the loads within a distance of  $0.5 d < a_v \leq 2 d$  may be reduced.

Finally, based on Eurocode 2 (EN 1992-1-1, 2004) for the closer load a punching capacity of 1392 kN resulted and for the further load a capacity of 796 kN.

According to Model code (CEB-FIP, 2013) the punching capacities followed to 717 kN and 632 kN for the closer and further load, respectively.

Detailed calculations can be found in Appendix D1 and Appendix D2.

#### 4.1.1.3 Flexural resistance

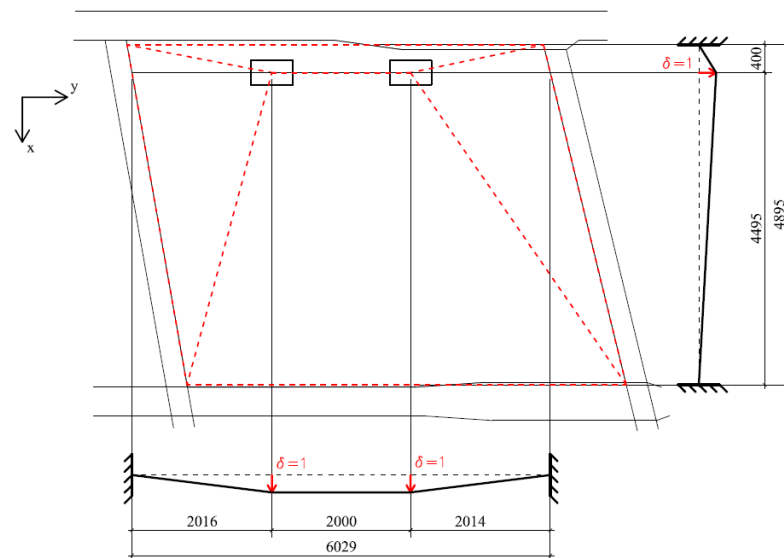


Figure 51: Yield line pattern by assuming a fully fixed slab.

The flexural resistance resulted to 2239 kN per loading plate by assuming a fully fixed slab. The derivation can be found in Appendix D3.

#### 4.1.1.4 Results & discussion

Table 9: Level I results by assuming a fully fixed slab.

Punching		One-way		Flexure	
Method	Capacity	Method	Capacity	Method	Capacity
EC	754 kN (CL)	EC	1392 kN (CL)	Yield line	2239 kN
	772 kN (FL)		796 kN (FL)		
MC	812 kN	MC	717 kN (CL)		
			632 kN (FL)		

\* CL = Closer loading point / FL = Further loading point



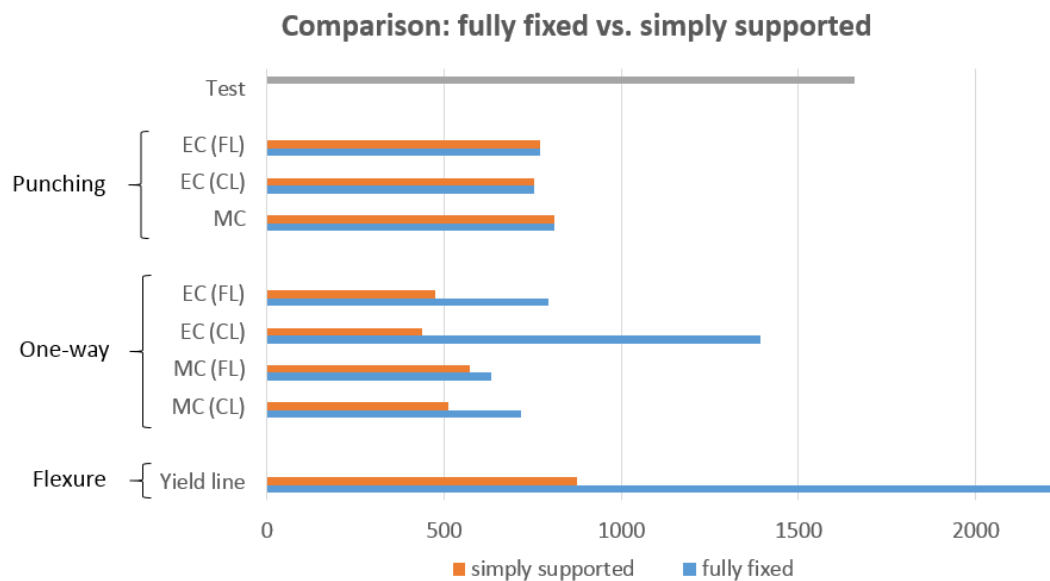


Figure 52: Comparison between fully fixed and simply supported slab for Level I assessment.

When comparing the results between a simply supported slab with a fully fixed slab, it is obvious that for punching the influence of boundary conditions was not considered. For one-way shear and flexure on the other hand, there resulted a big difference between these two assumptions.

Comparing the one-way resistance gained from a fully fixed slab with results obtained by assuming a simply supported slab, the difference in the results was very high. This came since by assuming a fully fixed slab in both Model code (CEB-FIP, 2013) and Eurocode 2 (EN 1992-1-1, 2004), the loads within a distance of  $0.5 d < a_v \leq 2 d$  may be reduced. In the current situation for the closer load in a distance of  $a_v = 155$  mm from the support, based on Eurocode 2 (EN 1992-1-1, 2004) the one-way shear resistance could be increased from 439 kN to 1392 kN. In Model code (CEB-FIP, 2013) on the other hand, the load could also be increased but only from 513 kN to 717 kN. In fact, in Model code (CEB-FIP, 2013) more advanced approximations exist. This means that for clamped slabs for instance, the load within a distance less than twice the effective depth may be reduced, but not more than to the half load ( $\beta \geq 0.5$ ). Further a distribution angle of  $\alpha = 45^\circ$  should be used for clamped slabs instead of an angle of  $\alpha = 60^\circ$  for simply supported slabs. Last but not least, the location of the control section is defined in Model code (CEB-FIP, 2013) to be in somewhere between the support and the loads. On the other hand in Eurocode 2 (EN 1992-1-1, 2004) nothing about the distribution angle as well as the location of the critical section is written.

Furthermore, it could be seen that by assuming a simply supported slab failure occurred at the closer load whereas by assuming a fully fixed slab it occurred at the further load. This may be connected with measurement inaccuracies.

For the flexural resistance it can be stated that for loads which act close to the support, boundary conditions have a big influence. This was because the angle between the loading point and the support reached in x-direction a high value (Figure 51) and that was why by applying the energy conservation principle a high value resulted for the forming yielding joint at the support.

## 4.1.2 Level II

### 4.1.2.1 Punching resistance

For Level II punching assessment, as mentioned in Chapter 3.2.3.2, the basic control perimeter  $b_1$  may be replaced by the shear-resisting control perimeter  $b_0$  and also the rotation factor  $\psi$  may be improved.

Since the rotation factors  $\psi_{II}$  and  $\psi_{III}$  compared to  $\psi_I$  only considers the bending resistance in addition, these parameters were the same as for a simply supported slab.

But on the other hand, the shear distribution around the loading plate and consequently the shear-resisting control perimeter varied. Figure 53 shows the shear distribution along the control perimeter with a maximal shear force of  $V_{perp,d,max} = 601$  kN due to an added load of  $V_{Ed} = 500$  kN. Finally, the shear-resisting control perimeter  $b_0$  followed to 0.83 m.

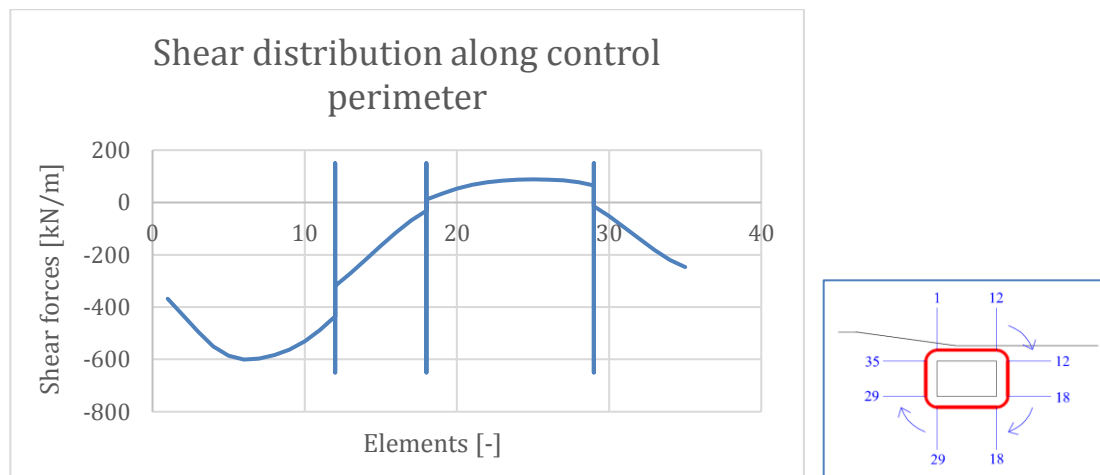


Figure 53: Shear distribution along control perimeter for a fully fixed slab.

As a result, based on the shear-resisting control perimeter  $b_0$ , punching capacities resulted to 260 kN, 75 kN and 91 kN by applying rotation factors  $\psi_I$  to  $\psi_{III}$ .

### 4.1.2.2 One-way shear resistance

In order to get the Level II one-way shear resistance, the analysis had been performed identically to Chapter 3.2.4. With an added load of  $V_d = 500$  kN per loading plate, an average shear force resistance along the critical width of  $v_d = 229$  kN/m resulted by assuming a fully fixed slab. Figure 54 shows the shear distribution along the critical section (blue line) and the average shear resistance along the critical width of 4.31 m (red line). The maximal peak comes from the load which was placed closer to the support.

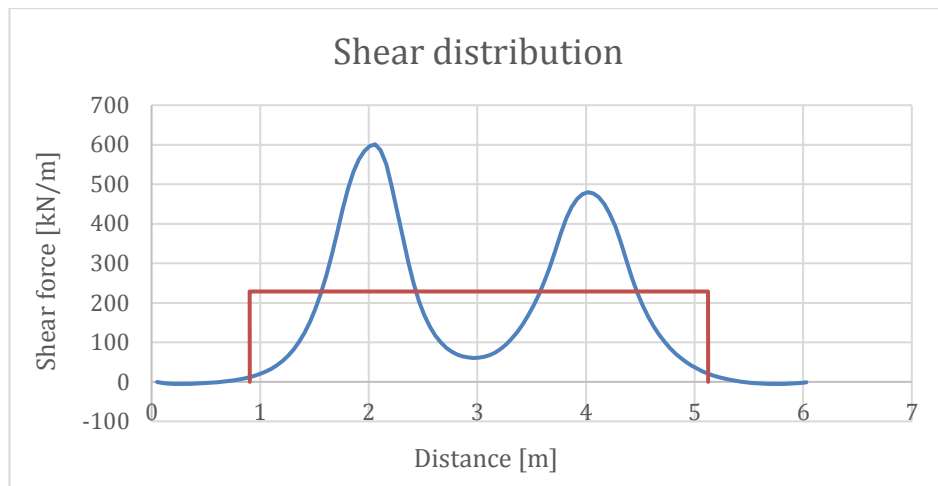


Figure 54: Shear force distribution along critical cross section (blue line) and distribution width with average value (red line).

The average shear force resistance based on Model code (CEB-FIP, 2013) in Level I assessment followed to  $632 \text{ kN} / 1.595 \text{ m} = 396 \text{ kN/m}$  and consequently, out of equation (25), a one-way shear resistance of  $V_{Rd} = 865 \text{ kN}$  resulted for Level II one-way shear assessment.

#### 4.1.2.3 Flexural resistance

For a fully fixed slab the application of the Swedish recommendation (Pacoste et al., 2012) delivered no valid flexure result, since in the current situation the critical section lied just next to the support, see Figure 28. Thus the bending value was negative along the critical section, see Figure 55, and that is why also a calculated flexural resistance according to equation (26) had been resulted in an unrealistic value.

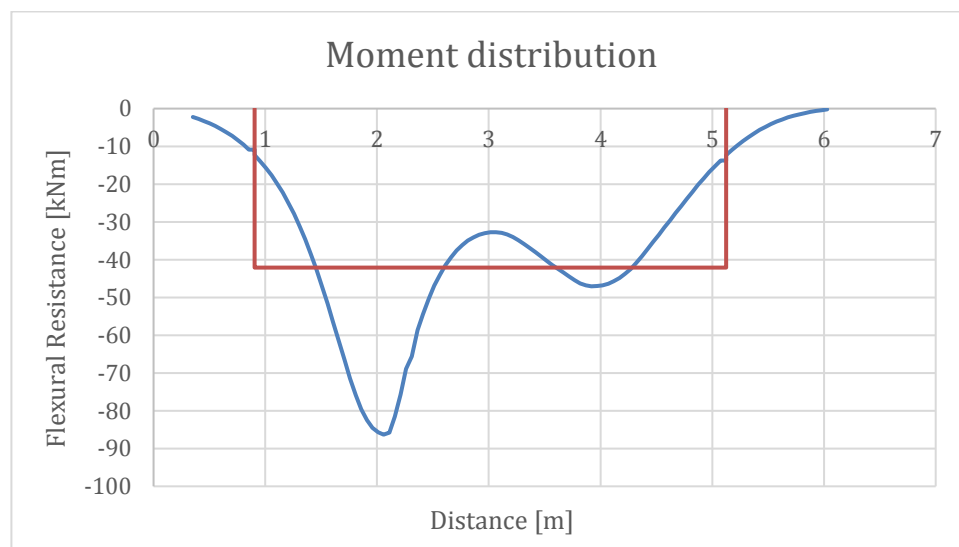


Figure 55: Moment distribution along critical cross section (blue line) and distribution width with average value (red line).

#### 4.1.2.4 Results & discussion

Table 10: Summary of results of Level II analysis.

Punching		One-way		Flexure	
Method	Capacity	Method	Capacity	Method	Capacity
MC ( $b_1$ )	233 kN ( $\psi_{II}$ )	Linearity properties	865 kN	Linearity properties	-
	286 kN ( $\psi_{III}$ )				
MC ( $b_0$ )	260 kN ( $\psi_I$ )				
	75 kN ( $\psi_{II}$ )				
	91 kN ( $\psi_{III}$ )				

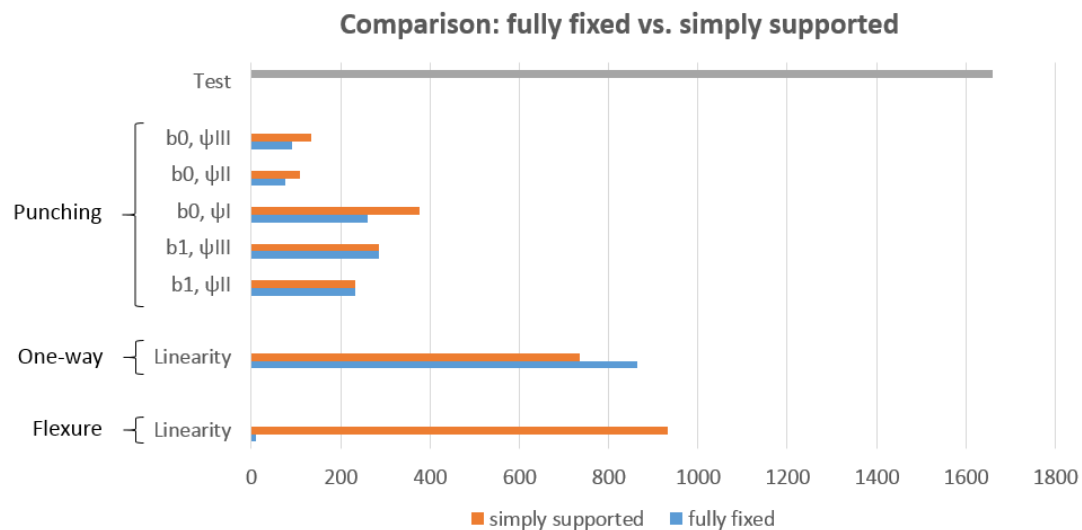


Figure 56: Comparison between fully fixed and simply supported slab for Level II assessment.

For the punching assessment it can be stated that the shear-resisting control perimeter  $b_0$  got an even lower value, if a fully fixed slab was assumed. This came since a fully fixed support can absorb even more shear force than a simple support. Consequently the maximal shear force per unit length perpendicular to the basic control perimeter ( $V_{perp,d,max}$ ) got higher and the shear-resisting control perimeter  $b_0$  got lower, according to equation (22).

For the one-way shear resistance according to equation (25), also a higher average shear force along the control perimeter led to a higher one-way shear resistance.

For the flexural resistance, as explained in Chapter 4.1.2.3, for a fully fixed slab no realistic value resulted based on the Swedish recommendation (Pacoste et al., 2012).

### 4.1.3 Level III

#### 4.1.3.1 Punching resistance

For Level III punching assessment the critical shear crack theory was applied (Chapter 3.3.3). The parameters used for a fully supported slab were the same as for the simply supported slab and are listed in Table 7.

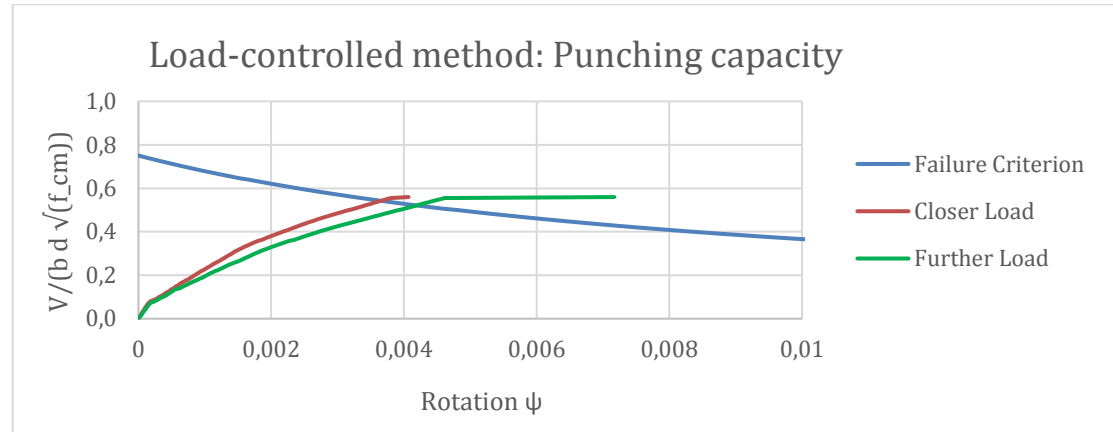


Figure 57: Punching capacity for fully fixed slab calculated based on the load-controlled method.

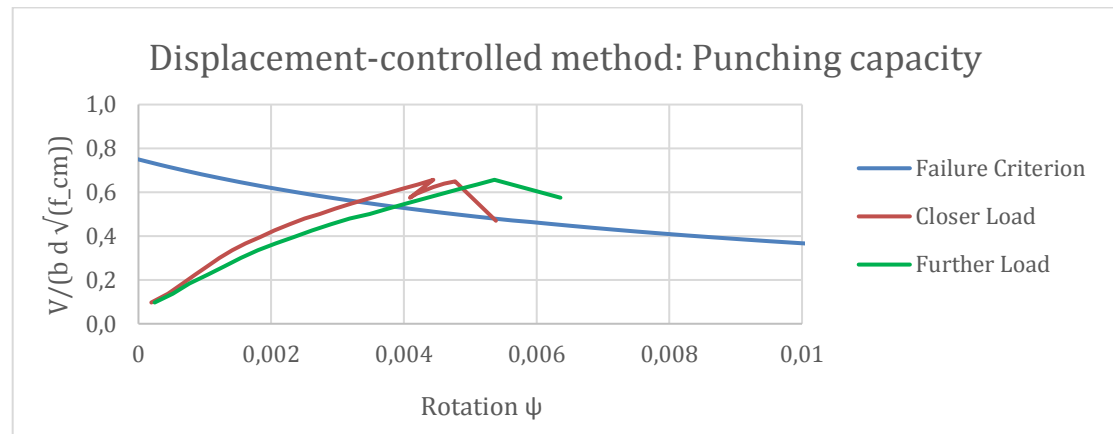


Figure 58: Punching capacity for fully fixed slab calculated based on the displacement-controlled method.

Analyses based on the load-controlled method provided for a fully fixed slab a punching capacity of 2482 kN for the closer load and a capacity of 2388 kN for the further load.

Analyses performed with the displacement-controlled method delivered punching capacities of 2548 kN for the closer and 2445 kN for the further load, respectively.

#### 4.1.3.2 Flexural resistance

For determining the flexural resistance, the load-displacement curves were analysed until failure occurred. This was possible, since shell elements reflect only bending failure.

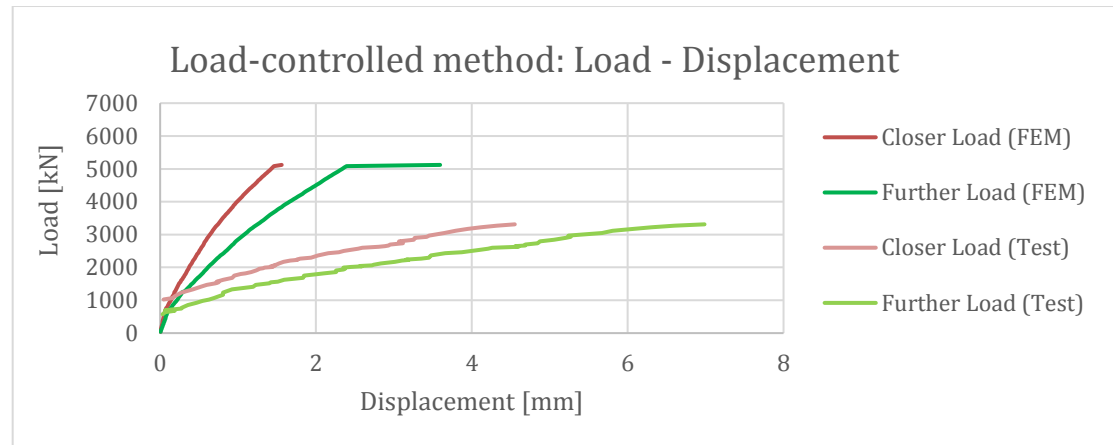


Figure 59: Load-displacement curves for fully fixed slab based on the load-controlled method.

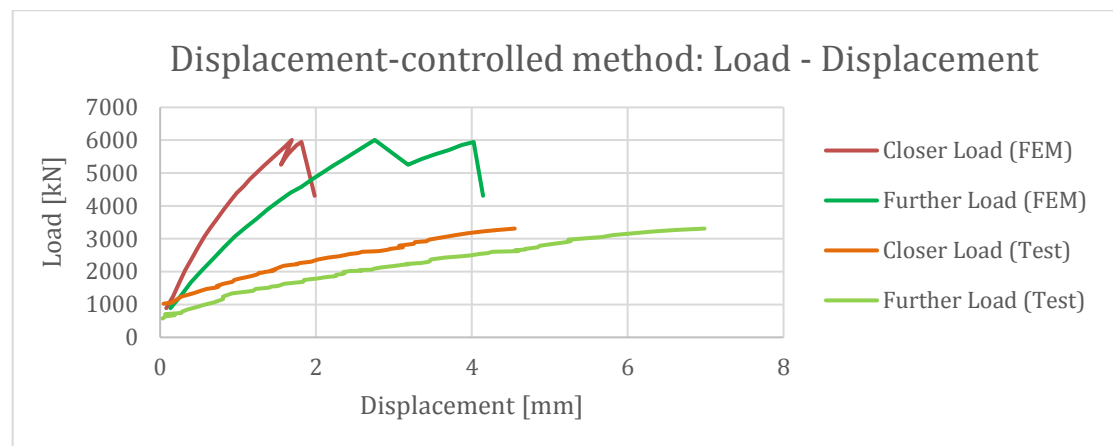


Figure 60: Load-displacement curves for fully fixed slab based on the displacement-controlled method.

The flexural resistance was reached by an added load of 5120 kN according to the load-controlled method and by an added load of 6010 kN according to the displacement-controlled method. These loads represented the total applied load, which means the load for both loading plates.

#### 4.1.3.3 Results & discussion

Table 11: Summary of results of Level II analysis.

Punching		One-way		Flexure	
Method	Capacity	Method	Capacity	Method	Capacity
CSCT (LM)	2482 kN (CL)	-	-	Non-lin. FE (LM)	2560 kN
	2388 kN (FL)				
CSCT (DM)	2548 kN (CL)			Non-lin. FE (DM)	3005 kN
	2445 kN (FL)				

\* CL = Closer loading point / FL = Further loading point

LM = Load-controlled method / DM = Displacement-controlled method

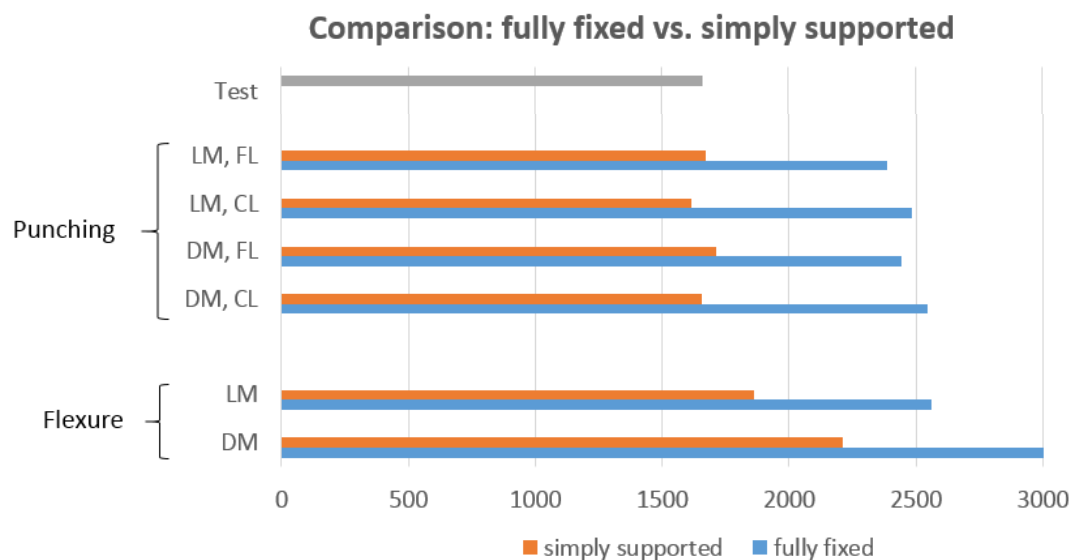


Figure 61: Comparison between fully fixed and simply supported slab for Level III assessment.

It can be stated that an assumption of a fully fixed slab delivered about 50 % higher values for the punching resistance compared to a simply supported slab.

Furthermore, by comparing the punching results gained with the two different boundary conditions, it can be stated that for a fully fixed slab the further load was decisive, whereas for a simply supported slab it was the closer load.

For the flexural resistance the displacement-controlled method delivered more conservative values as the load-controlled method. However, both values were higher than the punching resistance.

## 4.2 Influence of effective depth

Since the thickness of the slab varied below the loading point, also the thickness along the control perimeter changed. As for punching, actually, the effective depth along the critical section should be considered, it was interesting to evaluate the influence of the effective depth on the punching capacity. Therefore, the punching resistance was calculated for effective depths of  $d = 203$  mm,  $d = 223$  mm and  $d = 243$  mm. As seen in Figure 62, these heights represented the effective depths along the left side of the control perimeter, in the middle and along the right side of the control perimeter.

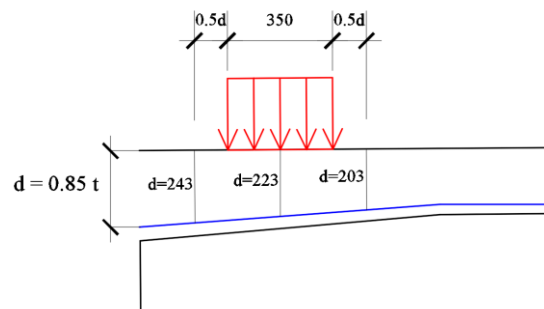


Figure 62: Effective depth below the middle of the loading point as well as below the borders of the control perimeter.

In this chapter only Level III punching assessment according to the critical shear crack theory was performed. Thereby, the two boundary conditions simply supported as well as fully fixed were investigated.

### 4.2.1 Punching capacity

Figure 63 and Figure 64 show the application of the critical shear crack theory for a simply supported slab and for a fully fixed slab, respectively. Non-linear FE analyses were performed based on the load-controlled method.

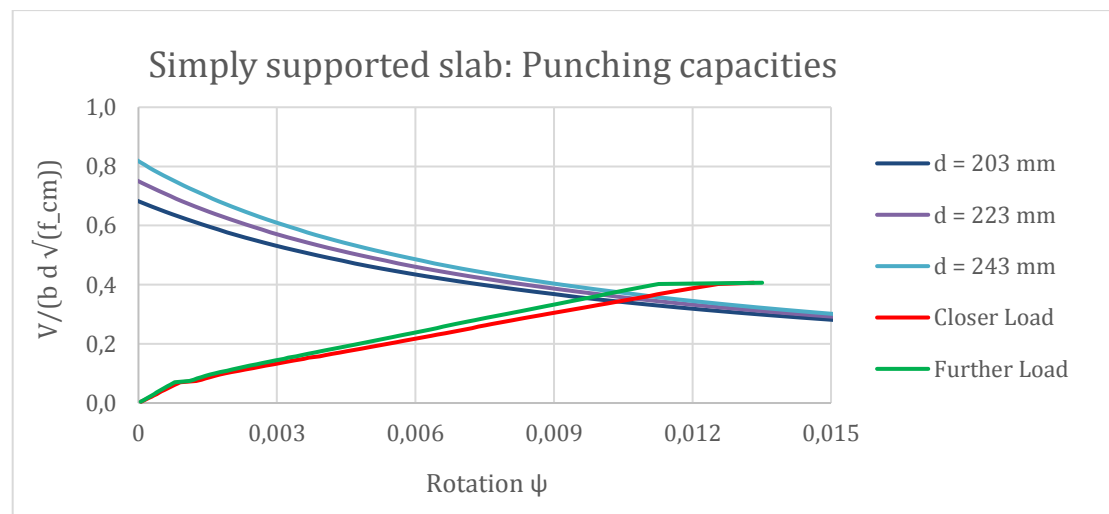


Figure 63: Influence of effective depth on the punching capacity for simply supported slab.



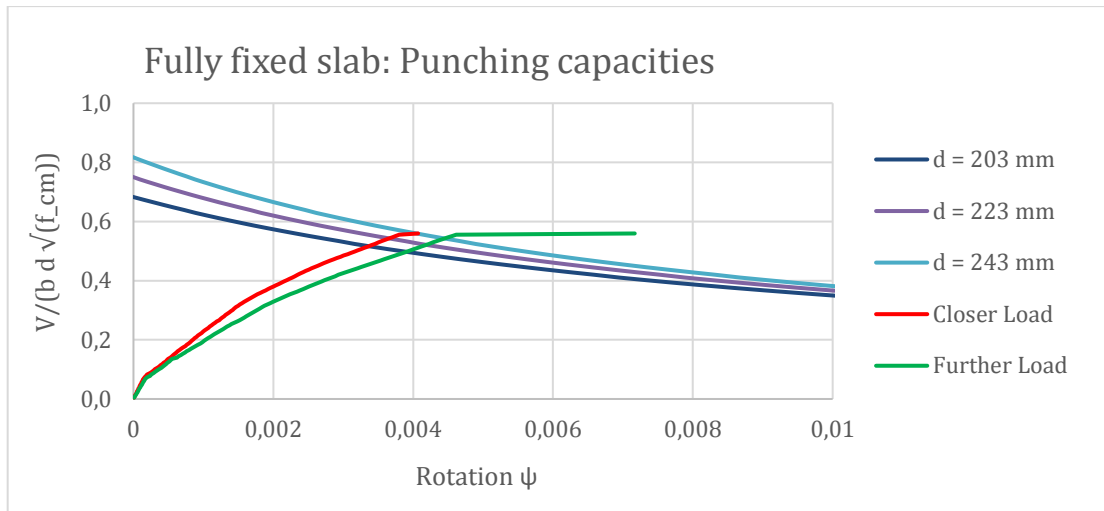


Figure 64: Influence of effective depth on the punching capacity for fully fixed slab.

The gained results are summarised and discussed in Chapter 4.2.2.

## 4.2.2 Results & discussion

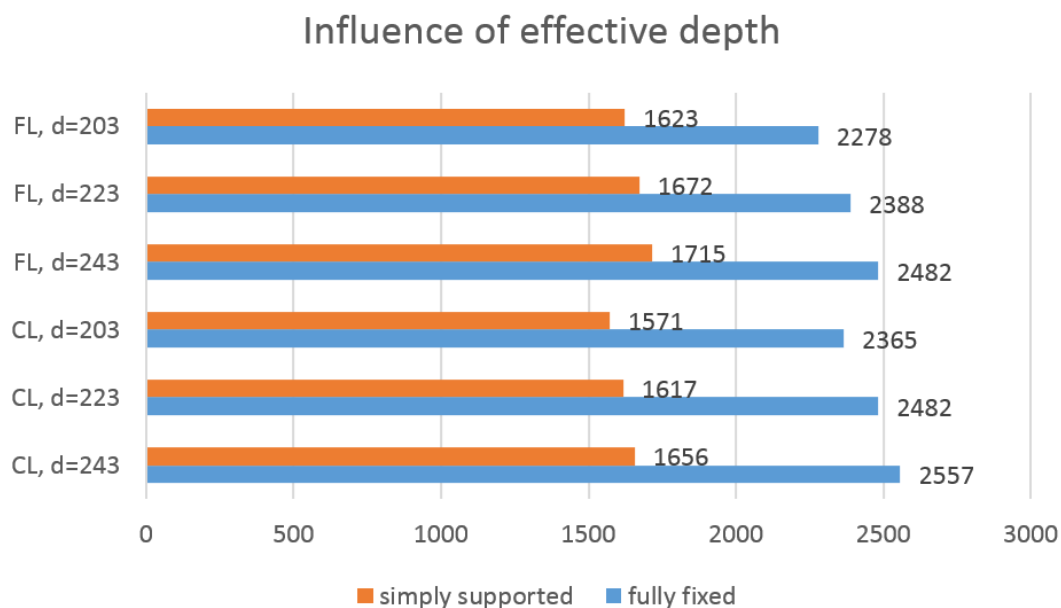


Figure 65: Influence of the effective depth on the punching capacity.

In general, it can be noted that the punching capacity increased by raising the effective depth. This was as expected, since with an increased effective depth the area is increased which can absorb the added shear force.

Comparing the results for a fully fixed slab with a simply supported slab, it can be noticed that a variation of the effective depth had a bigger influence for a fully fixed slab. But in conclusion, the difference in the punching capacity was very small by varying the effective depth.

## 5 Conclusions

Based on performed studies the following conclusions can be drawn:

- First of all it can be concluded that the multi-level assessment strategy provided successively improved evaluation in structural assessment. Nevertheless there was an exception for the Level II punching resistance which delivered less accurate results than Level I assessment.
- For the underestimation of the punching capacity at Level II there might be two reasons. First, the low reinforcement ratio below the loading points provided a small bending resistance of the slab and finally a small value for the punching resistance. Second, due to the predominate shear distribution to the outside girder, an immense value for the maximal shear along the control perimeter resulted and consequently an unrealistic small value for the shear-resisting perimeter  $b_0$ .
- The shear-resisting control perimeter  $b_0$  did not provide accurate results if the concentrated load was placed close to the support. As mentioned above, this was caused due to an unsymmetrical shear distribution around the loads.
- For simple hand-calculations regarding shear assessment Model code (CEB-FIP, 2013) delivered more advanced assumptions than Eurocode 2 (EN 1992-1-1, 2004). Especially by taking a control perimeter in a distance of twice the effective depth into account, in Eurocode 2 (EN 1992-1-1, 2004) reinforcement was considered which actually cannot absorb the loads. Furthermore, for one-way shear calculations, in Eurocode 2 (EN 1992-1-1, 2004) the distribution angle as well as the location of the critical section were not defined.
- For Level II assessment based on the Swedish recommendation (Pacoste et al., 2012), its application was only available if moment distribution did not vary immense between the point of load and the critical section. As seen for a fully fixed slab the moment distribution changed from negative values at the support to positive values below the load. In this case instead of a positive moment value a negative value was considered and that was why no right results were gained.
- The application of shell elements for the FE analysis in combination with the critical shear crack theory delivered accurate results. However, especially if loads were placed close to the support, the gained results have to be evaluated critically. An appropriate choice of boundary conditions was crucial.
- A parameter study showed that the effective depth did not have a big influence on the punching capacity. Thus for future investigations it will be a reasonable assumption to use the average effective depth below the centre of the load.

- By analysing the influence of boundary conditions, it was shown that a fully fixed slab delivered an approximately 50 % higher load carrying capacity. Thus it could be stated that boundary conditions have the biggest influence on the punching capacity if loads were placed close to the support. This influence was even more pronounced, the closer the load was placed to the support.
- By analysing the two loading points separately, it was shown that by assuming a simply supported slab punching failure occurred at the closer load, but by assuming a fully fixed slab it occurred at the further load. However, the failure happened below the further load in the test. The reason for this may be found in measurement inaccuracies since for both loading plates the calculated load carrying capacities varied minimally.

## 6 Future study

In a next step based on the multi-level assessment strategy, Level IV and V assessments are suggested to be performed. These analyses should be done with 3D continuum elements which can reflect shear type failures including punching (Plos et al., 2015). In addition for Level V assessment, the bond-slip behaviour of the interface between the reinforcement and the concrete will be also included (Plos et al., 2015).

For future studies regarding the Kiruna Bridge, it is suggested to investigate why in the test punching failure occurred at the further loading point; whereas based on the FE analysis it was expected to take place at the closer load. Since for assuming a fully fixed slab the decisive load had been also the further one, may the reason lay in the boundary conditions. Or perhaps there are other mechanisms which were not considered within this thesis?

An interesting point may also be the investigation and description of the mutual influence of the two loading plates. Since the distance between their centres was 2.0 m, it could be assumed that punching failure occurred either below the closer load or the further load. On the other hand, in a previous master's thesis (Ashraf & Hasan, 2015) the two loading plates were placed in a distance of 0.9 m between their centres and punching occurred over the whole area including the two loading points plus the area in between. In conclusion, it would be interesting to evaluate in which case failure occurs only below one loading point and in which case punching failure occurs simultaneously over the whole area. Thus for a further study the distance between the centre of the two loads may be varied but also the dimensions of the loading plates.

Furthermore, it should be analysed in which way the mutual influence of the two loading plates can be considered. A certain consideration followed already since for the FE analysis the influence of both loads was considered but since shell elements cannot describe out of plane shear, it should be assessed if this consideration was enough.

Altogether it can be noticed that the CSCT represents a useful tool to determine the punching capacity in an accurate way. Nevertheless further studies, in particular full-scale tests, are suggested to be performed in order to verify the application of the CSCT.

## 7 References

- Ashraf, A., & Hasan, W. (2015): *Structural assessment of concrete bridge deck slabs using FEM*. Master's Thesis. Department of Structural Engineering and Building Technology, Chalmers University of Technology, Publication no. 15:143, Göteborg, Sweden, 2015, 90 pp.
- Bagge, N. (2014): *Assessment of Concrete Bridges*. Licentiate Thesis. Department of Structural Engineering, Luleå University of Technology, Luleå, Sweden, 2014, 132 pp.
- Bagge, N., Plos, M., Shu, J., & Elfgren, L. (2015): Punching Capacity of a Reinforced Concrete Bridge Deck Slab loaded to Failure. *Nordic Concrete Research*, no. 53, 57-60.
- Broo, H., Lundgren, K., & Plos, M. (2008): *A guide to non-linear finite element modelling of shear and torsion in concrete bridges*. Göteborg, Sweden.
- CEB-FIP. (2013): *fib Model Code for Concrete Structures 2010*. Lausanne, Switzerland.
- EN 1992-1-1. (2004): *Eurocode 2: Design of concrete structures - part 1-1: General rules and rules for buildings*. Brussels, Belgium: CEN European Committee for Standardization.
- Hakimi, P. S. (2012): *Distribution of Shear Force in Concrete Slabs*. Master's Thesis. Department of Structural Engineering and Building Performance Design, Chalmers University of Technology, Publication no. 12:148, Göteborg, Sweden, 2012, 94 pp.
- Muttoni, A. (2008): Punching Shear Strength of Reinforced Concrete Slabs without Transverse Reinforcement. *ACI Structural Journal*, (105), 440-450.
- Pacoste, C., Plos, M., & Johansson, M. (2012): *Recommendations for finite element analysis for the design of reinforced concrete slabs* (ISSN 1103-). Stockholm: TRITA-BKN Rapport 114, 55.
- Plos, M., Shu, J., Zandi, K., & Lundgren, K. (2015): A multi-level structural assessment proposal for reinforced concrete bridge deck slabs. *Structure and Infrastructure Engineering*, (2479), 1-19.
- TNO. (2014): *Diana finite element analysis, User's Manual -- Release 9.6*. TNO DIANA BV. Delft, Netherlands.

# Appendix A – Reinforcement Ratio

## A1) Reinforcement ratio of the slab

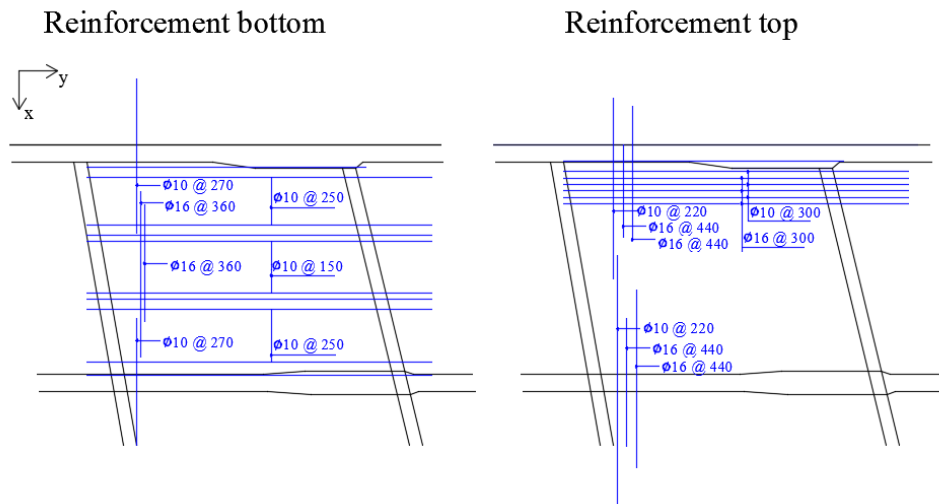


Figure 66: Bottom reinforcement layer (left) and top reinforcement layer (right).

Average thickness for a span of 5000 mm:  $t = 236 \text{ mm}$

### y-Direction

Bottom:

$$A_s = 24 \cdot \pi \cdot 5^2 = 1'885 \text{ mm}^2$$

$$A_c = 5000 \cdot 236 = 1'180'000 \text{ mm}^2$$

$$\rho_{y,b} = \frac{A_s}{A_c} = \frac{1'885}{1'180'000} = 0.160 \%$$

Top:

$$a_s = \frac{\pi \cdot 5^2}{0.3} + \frac{\pi \cdot 8^2}{0.3} = 932 \text{ mm}^2/\text{m}$$

$$a_c = 1000 \cdot 236 = 236'000 \text{ mm}^2/\text{m}$$

$$\rho_{y,t} = \frac{a_s}{a_c} = \frac{932}{236'000} = 0.395 \%$$

Total y-Direction:  $\rho_y = \rho_{y,b} + \rho_{y,t} = 0.56 \%$

## x-Direction

Bottom:  $A_s = \frac{\pi \cdot 5^2}{0.27} (1668 + 1328) + \frac{\pi \cdot 8^2}{0.36} (3908 + 2760) = 4'595'615 \text{ mm}^3$

$$A_c = 5000 \cdot 1000 \cdot 236 = 1'180'000'000 \text{ mm}^3$$

$$\rho_{x,b} = \frac{A_s}{A_c} = \frac{4'595'615}{1'180'000'000} = 0.389 \%$$

Top:  $A_s = \frac{\pi \cdot 5^2}{0.22} (2750 + 2795) + \frac{\pi \cdot 8^2}{0.44} (1779 + 1817 + 1311 + 1978) = 5'125'615 \text{ mm}^3$

$$A_c = 5000 \cdot 1000 \cdot 236 = 1'180'000'000 \text{ mm}^3$$

$$\rho_{x,t} = \frac{A_s}{A_c} = \frac{5'125'615}{1'180'000'000} = 0.434 \%$$

Total x-Direction:  $\rho_x = \rho_{x,b} + \rho_{x,t} = 0.82 \%$

Table 12: Summary reinforcement ratios.

y-Direction (bottom + top reinforcement)	$\rho_y = 0.56 \%$
x-Direction (bottom + top reinforcement)	$\rho_x = 0.82 \%$
Total bottom reinforcement	$\rho_b = 0.55 \%$
Total top reinforcement	$\rho_t = 0.84 \%$

## A2) Bottom reinforcement ratio inside control perimeter

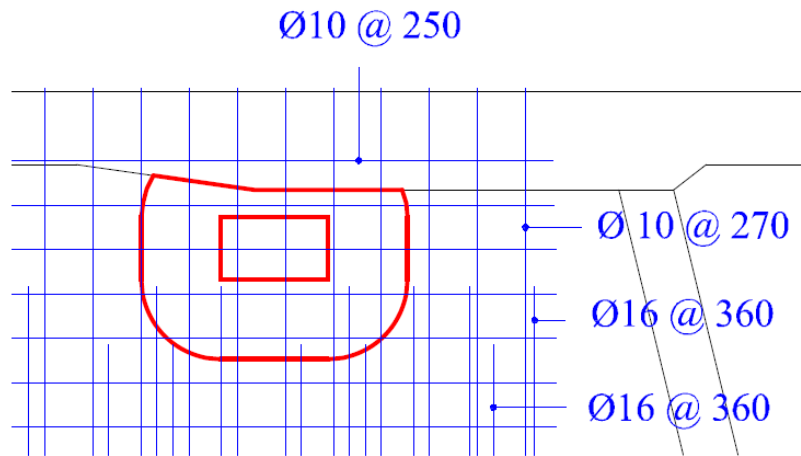


Figure 67: Bottom reinforcement inside control perimeter.

For the calculation in x-direction only the reinforcement was counted which extends over the whole distance.

Average thickness at the loading plate:  $t = 262 \text{ mm}$

### y-Direction

$$a_s = \frac{\pi \cdot 5^2}{0.25} = 314 \text{ mm}^2/\text{m}$$

$$a_c = 262 \cdot 1000 = 262'000 \text{ mm}^2/\text{m}$$

$$\rho_y = \frac{a_s}{a_c} = \frac{314}{262'000} = 0.120 \%$$

### x-Direction

$$a_s = \frac{\pi \cdot 5^2}{0.27} = 291 \text{ mm}^2/\text{m}$$

$$a_c = 262 \cdot 1000 = 262'000 \text{ mm}^2/\text{m}$$

$$\rho_x = \frac{a_s}{a_c} = \frac{291}{262'000} = 0.111 \%$$

$$\rho_l = \sqrt{\rho_y \cdot \rho_x} = 0.115 \%$$



### A3) Top reinforcement ratio along critical section

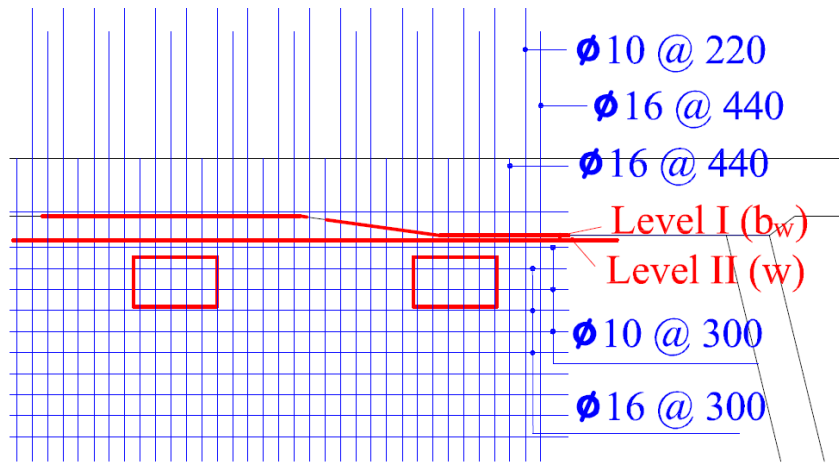


Figure 68: Top reinforcement along critical section.

Thickness along critical section Level I:  $t_I = 291 \text{ mm}$  ( $t_I = 300 \text{ mm}$ )

Thickness along critical section Level II:  $t_{II} = 286 \text{ mm}$

#### x-Direction

Level I:

$$a_s = \frac{\pi \cdot 5^2}{0.22} + 2 \frac{\pi \cdot 8^2}{0.44} = 1271 \text{ mm}^2/\text{m}$$

$$a_{c,I} = 291 \cdot 1000 = 291'000 \text{ mm}^2/\text{m}$$

$$\rho_{l,I} = \frac{a_s}{a_{c,I}} = \frac{1'271}{291'000} = 0.437 \%$$

Level II:

$$a_s = \frac{\pi \cdot 5^2}{0.22} + 2 \frac{\pi \cdot 8^2}{0.44} = 1271 \text{ mm}^2/\text{m}$$

$$a_{c,II} = 286 \cdot 1000 = 286'000 \text{ mm}^2/\text{m}$$

$$\rho_{l,II} = \frac{a_s}{a_{c,II}} = \frac{1'271}{286'000} = 0.444 \%$$

## Appendix B – Level I calculations

### B1) Punching based on Eurocode 2 (EN 1992-1-1, 2004)

---

Punching capacity:

$$V_{Rd,c} = v_{Rd,c} u d$$

Where:  $d \approx 0.85 \cdot t = 0.85 \cdot 262 = 223 \text{ mm}$   
 $u_1 = 4510 \text{ mm}$        $u_2 = 4614 \text{ mm}$       (Figure 14)  
 $v_{Rd,c} = 0.75 \text{ MPa}$  (\*)

Closer Load:  $V_{Rd,c,1} = v_{Rd,c} u_1 d = 0.75 \cdot 4510 \cdot 223 = 754 \text{ kN}$       decisive!

Further Load:  $V_{Rd,c,2} = v_{Rd,c} u_2 d = 0.75 \cdot 4614 \cdot 223 = 772 \text{ kN}$

---

#### (\*) Punching shear resistance of slabs without shear reinforcement

Design value (Eurocode 2)

$$v_{Rd,c} = C_{Rd,c} k (100 \rho_l f_{ck})^{1/3} + k_1 \sigma_{cp} \geq (v_{min} + k_1 \sigma_{cp}) \quad \text{EC2, (6.47)}$$

$$v_{min} = 0.035 k^{3/2} f_{ck}^{1/2} \quad \text{EC2, (6.3N)}$$

Average value:

$$v_{Rd,c} = 0.18 k (100 \rho_l f_{cm})^{1/3} + k_1 \sigma_{cp}$$

$$v_{min} = 0.035 k^{3/2} f_{cm}^{1/2}$$

Where:  $k = 1 + \sqrt{\frac{200}{d}} = 1 + \sqrt{\frac{200}{223}} = 1.95 \leq 2.0$  o.k.  
 $\rho_l = 0.12 \% \leq 2 \%$       (Appendix A2)  
 $f_{cm} = 62.2 \text{ MPa}$   
 $\sigma_{cp} = 0$

$$v_{Rd,c} = C_{Rd,c} k (100 \rho_l f_{cm})^{1/3} = 0.18 \cdot 1.95 \cdot (100 \cdot 0.0012 \cdot 62.2)^{1/3} = 0.69 \text{ MPa}$$

$$v_{min} = 0.035 k^{3/2} f_{cm}^{1/2} = 0.035 \cdot 1.95^{3/2} \cdot 62.2^{1/2} = 0.75 \text{ MPa}$$

## B2) Punching based on Model Code (CEB-FIP, 2013)

Punching capacity:

$$V_{Rd,c} = v_{Rd,c} b_1 d_v$$

Punching shear resistance of slabs without shear reinforcement

Design:  $v_{Rc,c} = k_\psi \frac{\sqrt{f_{ck}}}{\gamma_c}$  MC (7.3-61)

Average:  $v_{Rc,c} = k_\psi \sqrt{f_{cm}}$

$$k_\psi = \frac{1}{1.5 + 0.9 k_{dg} \psi d} = 0.274 < 0.6$$
 MC (7.3-63)

Level I approximation for rotation:  $\psi_I = 1.5 \frac{r_s f_{sm}}{d E_s}$

Input perimeter:

$$b_1 = 2601 \text{ mm}$$

$$d = 223 \text{ mm}$$

$$f_{cm} = 62.2 \text{ MPa}$$

$$k_{dg} = 1$$

$$f_{sm,t} = 584 \text{ MPa}$$

$$f_{sm,l} = 667 \text{ MPa}$$

$$E_s = 200 \text{ GPa}$$

Table 13: Punching capacity based on Model code with rotation factor  $\psi_I$ .

		L_1	L_2	L_3	L_4
L	(mm)	605	2165	4735	4171
r_s	(mm)	133	476	1042	918
f_sm	(Mpa)	584	667	584	667
d	(mm)	223	223	223	223
E_s	(Mpa)	200000	200000	200000	200000
$\psi_I$	(-)	0.0026	0.0107	0.0205	0.0206
k_ψ	(-)	0.493905	0.274392	0.178368	0.177577
V_Rd,c	(kN)	2259.4	1255.2	815.9	812.3

### B3) One-way shear based on Eurocode 2 (EN 1992-1-1, 2004)

---

Shear resistance for members not requiring design shear reinforcement:

$$V_{Rd,c} = v_{Rd,c} b_w d$$

Where:  $d \approx 0.85 \cdot t = 0.85 \cdot 289 = 246 \text{ mm}$   
 $b_{w,1} = 1731 \text{ mm}$        $b_{w,2} = 1883 \text{ mm}$       (Figure 17)  
 $v_{Rd} = 1.03 \text{ MPa}$

Closer Load:  $V_{Rd,c,1} = v_{Rd} b_{w,1} d = 1.03 \cdot 1731 \cdot 246 = 439 \text{ kN}$       decisive!

Further Load:  $V_{Rd,c,2} = v_{Rd} b_{w,2} d = 1.03 \cdot 1883 \cdot 246 = 477 \text{ kN}$

---

(\*) Shear resistance of members which do not requiring shear resistance

Design value:

$$v_{Rd,c} = C_{Rd,c} k (100 \rho_l f_{ck})^{1/3} + k_1 \sigma_{cp} \quad \text{EC2, (6.2.a)}$$

$$v_{Rd,c,min} = v_{min} + k_1 \sigma_{cp} \quad \text{EC2, (6.2.b)}$$

Average value:

$$v_{Rc,c} = 0.18 k (100 \rho_l f_{cm})^{1/3} + k_1 \sigma_{cp}$$

$$v_{Rd,c,min} = 0.035 k^{3/2} f_{cm}^{1/2} + k_1 \sigma_{cp}$$

Where:  $k = 1 + \sqrt{\frac{200}{d}} = 1 + \sqrt{\frac{200}{246}} = 1.90 \leq 2,0$       o.k.  
 $\rho_l = 0.44 \% \leq 2 \%$       o.k.      (Appendix A3)  
 $f_{cm} = 62.2 \text{ MPa}$   
 $\sigma_{cp} = 0$

$$v_{Rc,c} = 0.18 k (100 \rho_l f_{cm})^{1/3} = 0.18 \cdot 1.90 \cdot (100 \cdot 0.0044 \cdot 62.2)^{1/3} = 1.03 \text{ MPa}$$

$$v_{Rd,c,min} = 0.035 k^{3/2} f_{cm}^{1/2} = 0.035 \cdot 1.90^{3/2} \cdot 62.2^{1/2} = 0.72 \text{ MPa}$$

#### **B4) One-way shear based on Model code (CEB-FIP, 2013)**

---

Shear resistance for members not requiring design shear reinforcement:

$$V_{Rd,c} = v_{Rd,c} b_w z$$

Where:  $z \approx 0.80 \cdot t = 0.80 \cdot 280 = 224 \text{ mm}$   
 $b_{w,1} = 2080 \text{ mm}$        $b_{w,2} = 2323 \text{ mm}$       (Figure 18)  
 $v_{Rd} = 1.10 \text{ MPa}$

Closer Load:  $V_{Rd,c,1} = v_{Rd} b_{w,1} z = 1.10 \cdot 2080 \cdot 224 = \mathbf{513 \text{ kN}}$       decisive!

Further Load:  $V_{Rd,c,2} = v_{Rd} b_{w,2} z = 1.10 \cdot 2323 \cdot 224 = \mathbf{572 \text{ kN}}$

---

(\*) Shear resistance of slab without shear reinforcement

Design value:

$$v_{Rd,c} = k_v \frac{\sqrt{f_{ck}}}{\gamma_c} \quad \text{MC (7.3-17)}$$

Average value:

$$v_{Rd,c} = k_v \sqrt{f_{cm}}$$

Where:  $k_v = \frac{180}{1000 + 1.25z} = \frac{180}{1000 + 1.25 \cdot 224} = 0.14$   
 $f_{cm} = 62.2 \text{ MPa}$

$$v_{Rd,c} = k_v \sqrt{f_{cm}} = 0.14 \sqrt{62.2} = 1.10 \text{ MPa}$$

## B5) Flexural resistance

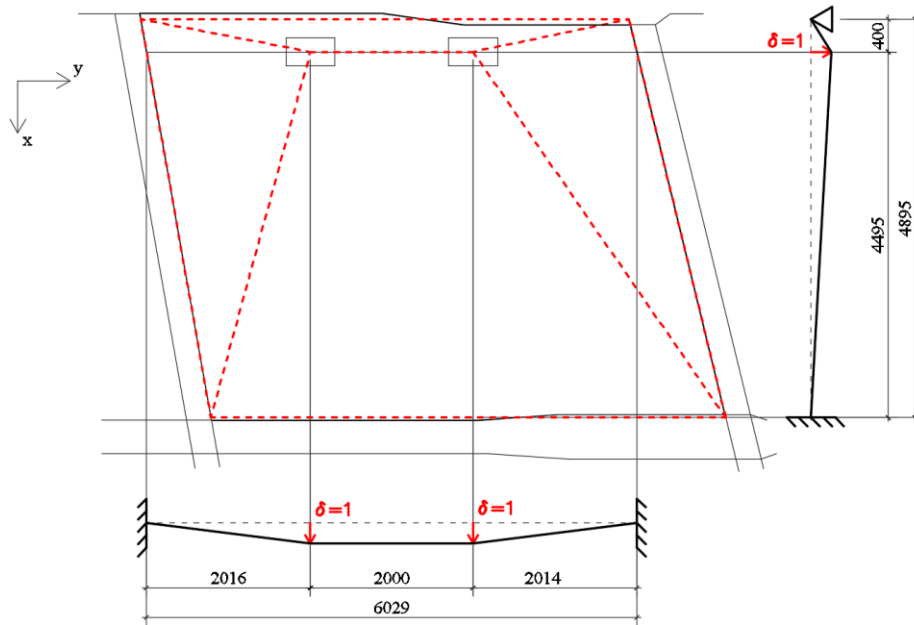


Figure 69: Yield line pattern.

Energy conservation principle:

$$Q \cdot \delta = m_{Rd} \cdot L \cdot \theta$$

Where:  $Q \cdot \delta = 2 \cdot Q$

$$m_{Rd} \cdot \theta \cdot L = m_{Rd,x} \cdot \theta_x \cdot L_y + m_{Rd,y} \cdot \theta_y \cdot L_x \quad \parallel m_{Rd} \rightarrow \text{Table 14}$$

x-Direction:

$$m_{Rd,x} \cdot \theta_x \cdot L_y = \left( 37.7 \cdot \left( \frac{1}{0.40} + \frac{1}{4.495} \right) + 183.4 \cdot \frac{1}{4.495} \right) 6.029 = 865 \text{ kN}$$

y-Direction:

$$m_{Rd,y} \cdot \theta_y \cdot L_x = \left( 135.5 \cdot \frac{1}{2.016} + 46.4 \cdot \frac{1}{2.016} + 46.4 \cdot \frac{1}{2.014} + 135.5 \cdot \frac{1}{2.014} \right) 4.895 = 884 \text{ kN}$$

$$2 \cdot Q = Q \cdot \delta = m_{Rd} \cdot \theta \cdot L = 1749 \text{ kN}$$

Per loading plate:  $V_{Rd} = 875 \text{ kN}$

Table 14: Flexural resistance at yield joints by assuming a fully fixed support.

Flexural Resistance											
			Reinforcement								
		Sector	Layer	ø [mm]	gap [mm]	a <sub>s</sub> [mm2]	d [mm]	f <sub>sm,t</sub> [MPa]	b [mm]	f <sub>cm</sub> [MPa]	m <sub>Rd</sub> [kNm/m]
x-Direction:	1	top		10	220	357					
				16	440	457					
				16	440	457					
						1271	250	584	1000	62.2	181.1
	2	bottom	10	270	291	223	584	1000	62.2	37.7	
	3	top		10	220	357					
				16	440	457					
				16	440	457					
						1271	253	584	1000	62.2	183.4
			Reinforcement								
		Sector	Layer	ø [mm]	gap [mm]	a <sub>s</sub> [mm2]	d	f <sub>sm,l</sub> [MPa]	b [mm]	f <sub>cm</sub> [MPa]	m <sub>Rd</sub> [kNm/m]
y-Direction:	4	top		10	300	262					
				16	300	670					
						932	223	667	1000	62.2	135.5
				5	bottom	10	250	314	223	667	1000
	6	top		10	300	262					
				16	300	670					
						932	223	667	1000	62.2	135.5

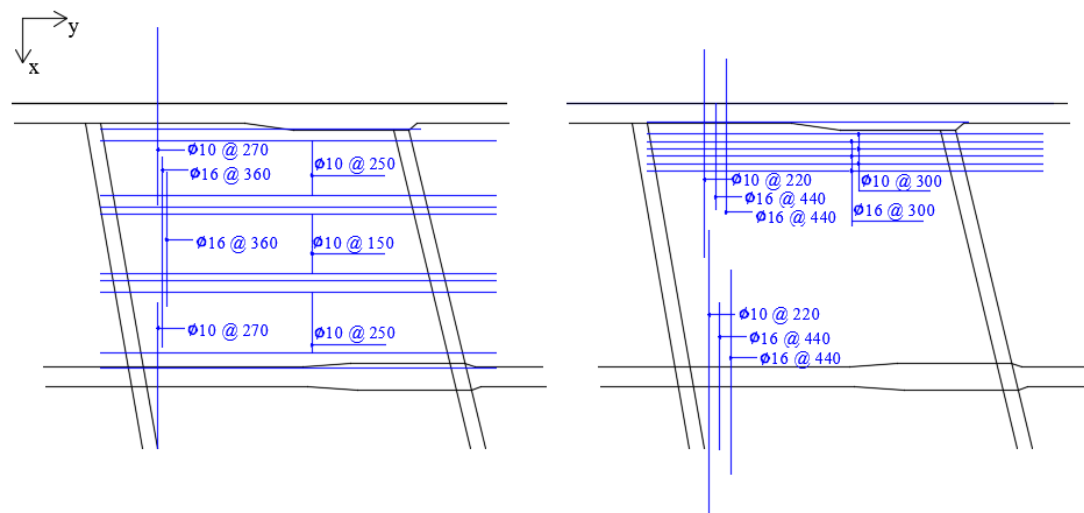


Figure 70: Bottom reinforcement ratio 0.55 % (left) and top reinforcement ratio 0.84 % (right).

## Appendix C – Level II calculations

### C1) Punching based on Model code (b1) (CEB-FIP, 2013)

Punching capacity:

$$V_{Rd,c} = v_{Rd,c} b_1 d_v$$

Punching shear resistance of slabs without shear reinforcement

Design:  $v_{Rc,c} = k_\psi \frac{\sqrt{f_{ck}}}{\gamma_c}$  MC (7.3-61)

Average:  $v_{Rc,c} = k_\psi \sqrt{f_{cm}}$

$$k_\psi = \frac{1}{1.5 + 0.9 k_{dg} \psi d} = 0.274 < 0.6$$
 MC (7.3-63)

Level II approximation for rotation:  $\psi_{II} = 1.5 \frac{r_s f_{sm}}{d E_s} \left( \frac{m_{Ed}}{m_{Rd}} \right)^{1.5}$

Level III approximation for rotation:  $\psi_{III} = 1.2 \frac{r_s f_{sm}}{d E_s} \left( \frac{m_{Ed}}{m_{Rd}} \right)^{1.5}$

Input perimeter:  $b_1 = 2601 \text{ mm}$

$$d = 223 \text{ mm}$$

$$f_{cm} = 62.2 \text{ MPa}$$

$$k_{dg} = 1$$

$$f_{sm,t} = 584 \text{ MPa}$$

$$f_{sm,t} = 667 \text{ MPa}$$

$$E_s = 200 \text{ GPa}$$

$$m_{Ed} \cong V_d / 8 = 812 / 8 = 101.5 \text{ kN}$$

$$m_{Rd,x} = 37.7 \text{ kN}$$

$$m_{Rd,y} = 46.4 \text{ kN}$$

Bending resistance m_Rd			x-Direction		y-Direction	
$m_{Rd} = \alpha_s f_{sm} z = \alpha_s f_{sm} \left( d - \frac{\alpha_s f_{sm}}{2b f_{cm}} \right)$			f_sm	584 Mpa	f_sm	667 Mpa
d	223 mm		diameter	10 mm	diameter	10 mm
b	1000 mm		distance	270 mm	distance	250 mm
f_cm	62.2 Mpa		a_s	291 mm <sup>2</sup> /m	a_s	314 mm <sup>2</sup> /m
			m_Rd	37.7 kN	m_Rd	46.4 kN

Figure 71: Bending resistance below loading plates.



Table 15: Punching capacity based on Model code with  $b_1$  and rotation factor  $\psi_{II}$ .

		<b>L_1</b>	<b>L_2</b>	<b>L_3</b>	<b>L_4</b>
L	(mm)	605	2165	4735	4171
r_s	(mm)	133	476	1042	918
f_ym	(Mpa)	584	667	584	667
d	(mm)	223	223	223	223
E_s	(Mpa)	200000	200000	200000	200000
m_Ed	(kN)	101.5	101.5	101.5	101.5
m_Rd	(kN)	37.7	46.4	37.7	46.4
$\psi_{II}$	(-)	0.0115	0.0346	0.0904	0.0666
k_ψ_II	(-)	0.261929	0.118512	0.050916	0.067266
<b>V_Rd,c</b>	<b>(kN)</b>	<b>1198.2</b>	<b>542.1</b>	<b>232.9</b>	<b>307.7</b>

Table 16: Punching capacity based on Model code with  $b_1$  and rotation factor  $\psi_{III}$ .

		<b>L_1</b>	<b>L_2</b>	<b>L_3</b>	<b>L_4</b>
L	(mm)	605	2165	4735	4171
r_s	(mm)	133	476	1042	918
f_ym	(Mpa)	584	667	584	667
d	(mm)	223	223	223	223
E_s	(Mpa)	200000	200000	200000	200000
m_Ed	(kN)	101.5	101.5	101.5	101.5
m_Rd	(kN)	37.7	46.4	37.7	46.4
$\psi_{III}$	(-)	0.0092	0.0277	0.0723	0.0533
k_ψ_III	(-)	0.29813	0.14184	0.06245	0.08201
<b>V_Rd,c</b>	<b>(kN)</b>	<b>1363.8</b>	<b>648.8</b>	<b>285.7</b>	<b>375.2</b>

## C2) Punching based on Model code (b<sub>0</sub>) (CEB-FIP, 2013)

Punching capacity:

$$V_{Rd,c} = v_{Rd,c} b_0 d_v$$

Punching shear resistance of slabs without shear reinforcement

Design:  $v_{Rc,c} = k_\psi \frac{\sqrt{f_{ck}}}{\gamma_c}$  MC (7.3-61)

Average:  $v_{Rc,c} = k_\psi \sqrt{f_{cm}}$

$$k_\psi = \frac{1}{1.5 + 0.9 k_{dg} \psi d} = 0.274 < 0.6$$
 MC (7.3-63)

Level I approximation for rotation:  $\psi_I = 1.5 \frac{r_s f_{sm}}{d E_s}$

Level II approximation for rotation:  $\psi_{II} = 1.5 \frac{r_s f_{sm}}{d E_s} \left( \frac{m_{Ed}}{m_{Rd}} \right)^{1.5}$

Level III approximation for rotation:  $\psi_{III} = 1.2 \frac{r_s f_{sm}}{d E_s} \left( \frac{m_{Ed}}{m_{Rd}} \right)^{1.5}$

Input perimeter:  $b_0 = 1208 \text{ mm}$

$$d = 223 \text{ mm}$$

$$f_{cm} = 62.2 \text{ MPa}$$

$$k_{dg} = 1$$

$$f_{sm,t} = 584 \text{ MPa}$$

$$f_{sm,t} = 667 \text{ MPa}$$

$$E_s = 200 \text{ GPa}$$

$$m_{Ed} \cong V_d/8 = 812/8 = 101.5 \text{ kN}$$

$$m_{Rd,x} = 37.7 \text{ kN}$$

$$m_{Rd,y} = 46.4 \text{ kN}$$

Bending resistance m_Rd			x-Direction		y-Direction	
$m_{Rd} = a_s f_{sm} z = a_s f_{sm} \left( d - \frac{a_s f_{sm}}{2b f_{cm}} \right)$			f_sm	584 Mpa	f_sm	667 Mpa
			diameter	10 mm	diameter	10 mm
d	223 mm		distance	270 mm	distance	250 mm
b	1000 mm		a_s	291 mm <sup>2</sup> /m	a_s	314 mm <sup>2</sup> /m
f_cm	62.2 MPa		m_Rd		m_Rd	46.4 kN
			37.7 kN			

Figure 72: Bending resistance below loading plates.

Table 17: Punching capacity based on Model code with  $b_0$  and rotation factor  $\psi_I$ .

		L_1	L_2	L_3	L_4
L	(mm)	605	2165	4735	4171
r_s	(mm)	133	476	1042	918
f_sm	(Mpa)	584	667	584	667
d	(mm)	223	223	223	223
E_s	(Mpa)	200000	200000	200000	200000
$\psi_I$	(-)	0.0026	0.0107	0.0205	0.0206
k_ψ	(-)	0.493905	0.274392	0.178368	0.177577
V_Rd,c	(kN)	1049.3	583.0	379.0	377.3

Table 18: Punching capacity based on Model code with  $b_0$  and rotation factor  $\psi_{II}$ .

		L_1	L_2	L_3	L_4
L	(mm)	605	2165	4735	4171
r_s	(mm)	133	476	1042	918
f_ym	(Mpa)	584	667	584	667
d	(mm)	223	223	223	223
E_s	(Mpa)	200000	200000	200000	200000
m_Ed	(kN)	101.5	101.5	101.5	101.5
m_Rd	(kN)	37.7	46.4	37.7	46.4
$\psi_{II}$	(-)	0.0115	0.0346	0.0904	0.0666
k_ψ_II	(-)	0.261929	0.118512	0.050916	0.067266
V_Rd,c	(kN)	556.5	251.8	108.2	142.9

Table 19: Punching capacity based on Model code with  $b_0$  and rotation factor  $\psi_{III}$ .

		<b>L_1</b>	<b>L_2</b>	<b>L_3</b>	<b>L_4</b>
L	(mm)	605	2165	4735	4171
r_s	(mm)	133	476	1042	918
f_ym	(Mpa)	584	667	584	667
d	(mm)	223	223	223	223
E_s	(Mpa)	200000	200000	200000	200000
m_Ed	(kN)	101.5	101.5	101.5	101.5
m_Rd	(kN)	37.7	46.4	37.7	46.4
$\psi_{III}$	(-)	0.0092	0.0277	0.0723	0.0533
k_ψ_III	(-)	0.298128	0.141836	0.062452	0.082013
<b>V_Rd,c</b>	<b>(kN)</b>	<b>633.4</b>	<b>301.3</b>	<b>132.7</b>	<b>174.2</b>

### C3) Critical section of the slab according to Swedish recommendation (Pacoste et al., 2012)

---

Distance to critical section of the slab:

$$y_{cs} = \frac{c + d}{2}$$

Where:  $c = 350$   
 $d = 244$

$$y_{cs} = \frac{c + d}{2} = \frac{350 + 244}{2} = 297 \text{ mm}$$

Width of the critical section:

$$w = \min(7d + b + t; 10d + 1.3y_{cs}) \quad \text{for } y = y_{max}$$

$$w_1 = 7d + b + t = 7 \cdot 244 + 600 + 0 = 2308 \text{ mm} \quad \text{decisive!}$$

$$w_2 = 10d + 1.3y_{cs} = 10 \cdot 244 + 1.3 \cdot 297 = 2826 \text{ mm}$$

$$\rightarrow w = 2308 \text{ mm}$$

## Appendix D – Parameter study - BC

### D1) One-way shear based on Eurocode 2 (EN 1992-1-1, 2004)

---

Shear resistance for members not requiring design shear reinforcement:

$$V_{Rd,c} = v_{Rd,c} b_w d$$

Where:

$$\begin{aligned} d &\approx 0.85 \cdot t = 0.85 \cdot 289 = 246 \text{ mm} \\ b_{w,1} &= 1731 \text{ mm} & b_{w,2} &= 1883 \text{ mm} & (\text{Figure 17}) \\ v_{Rd,1} &= 3.27 \text{ MPa} & v_{Rd,2} &= 1.72 \text{ MPa} (*) \end{aligned}$$

Closer Load:  $V_{Rd,c,1} = v_{Rd,1} b_{w,1} d = 3.27 \cdot 1731 \cdot 246 = \mathbf{1392 \text{ kN}}$

Further Load:  $V_{Rd,c,2} = v_{Rd,2} b_{w,2} d = 1.72 \cdot 1883 \cdot 246 = \mathbf{796 \text{ kN}}$  decisive!

---

#### (\*) Shear resistance of members which do not requiring shear resistance

Design value:

$$v_{Rd,c} = C_{Rd,c} k (100 \rho_l f_{ck})^{1/3} + k_1 \sigma_{cp} \quad \text{EC2, (6.2.a)}$$

$$v_{Rd,c,min} = v_{min} + k_1 \sigma_{cp} \quad \text{EC2, (6.2.b)}$$

Average value:

$$v_{Rc,c} = 0.18 k (100 \rho_l f_{cm})^{1/3} + k_1 \sigma_{cp}$$

$$v_{Rd,c,min} = 0.035 k^{3/2} f_{cm}^{1/2} + k_1 \sigma_{cp}$$

Where:

$$\begin{aligned} k &= 1 + \sqrt{\frac{200}{d}} = 1 + \sqrt{\frac{200}{246}} = 1.90 \leq 2.0 \quad \text{o.k.} \\ \rho_l &= 0.44 \% \leq 2 \% \quad \text{o.k.} \\ f_{cm} &= 62.2 \text{ MPa} \\ \sigma_{cp} &= 0 \end{aligned} \quad (\text{Appendix A3})$$

$$v_{Rc,c} = 0.18 k (100 \rho_l f_{cm})^{1/3} = 0.18 \cdot 1.90 \cdot (100 \cdot 0.0044 \cdot 62.2)^{1/3} = 1.03 \text{ MPa}$$

$$v_{Rd,c,min} = 0.035 k^{3/2} f_{cm}^{1/2} = 0.035 \cdot 1.90^{3/2} \cdot 62.2^{1/2} = 0.72 \text{ MPa}$$

Assuming that the longitudinal reinforcement is fully anchored at the support, a load within a distance of  $0.5d < a_v \leq 2d$  may be reduced:

$$\beta = a_v / (2d) \quad \text{EC, 6.2.2 (6)}$$

Closer Load:

$$\beta_1 = a_{v,1} / (2d) = 155 / (2 \cdot 246) = 0.315$$

$$v_{Rd,1} = v_{Rd,c,alt} / \beta = 1.03 / 0.315 = 3.27 \text{ MPa}$$

Further Load:

$$\beta_2 = a_{v,2} / (2d) = 295 / (2 \cdot 246) = 0.600$$

$$v_{Rd,2} = v_{Rd,c,alt} / \beta = 1.03 / 0.600 = 1.72 \text{ MPa}$$

## D2) One-way shear based on Model code (CEB-FIP, 2013)

---

Shear resistance for members not requiring design shear reinforcement:

$$V_{Rd,c} = v_{Rd,c} b_w z$$

Where:  $z \approx 0.80 \cdot t = 0.80 \cdot 280 = 224 \text{ mm}$   
 $b_{w,1} = 1455 \text{ mm}$        $b_{w,2} = 1595 \text{ mm}$       (Figure 50)  
 $v_{Rd,1} = 2.20 \text{ MPa}$        $v_{Rd,2} = 1.77 \text{ MPa (*)}$

Closer Load:  $V_{Rd,c,1} = v_{Rd,1} b_w z = 2.20 \cdot 1455 \cdot 224 = 717 \text{ kN}$

Further Load:  $V_{Rd,c,2} = v_{Rd,2} b_w z = 1.77 \cdot 1595 \cdot 224 = 632 \text{ kN}$       decisive!

---

(\*) Shear resistance of slab without shear reinforcement

Design value:

$$v_{Rd,c} = k_v \frac{\sqrt{f_{ck}}}{\gamma_c} \quad \text{MC (7.3-17)}$$

Average value:

$$v_{Rd,c} = k_v \sqrt{f_{cm}}$$

Where:  $k_v = \frac{180}{1000 + 1.25z} = \frac{180}{1000 + 1.25 \cdot 224} = 0.14$   
 $f_{cm} = 62.2 \text{ MPa}$

$$v_{Rd,c} = k_v \sqrt{f_{cm}} = 0.14 \sqrt{62.2} = 1.10 \text{ MPa}$$

According to (7.3-13) may loads within a distance of  $0.5d < a_v \leq 2d$  from the face of the support be reduced:

$$\beta = a_v / (2d) \quad \text{MC (7.3-13)}$$

Closer Load:

$$a_v = 155 < d = 238 \rightarrow \beta_1 = 0.5$$
$$v_{Rd,1} = v_{Rd,c,alt} / \beta_1 = 1.10 / 0.5 = 2.20 \text{ MPa}$$

Further Load:

$$\beta_2 = a_{v,2} / (2d) = 295 / (2 \cdot 238) = 0.620$$
$$v_{Rd,2} = v_{Rd,c,alt} / \beta_2 = 1.10 / 0.620 = 1.77 \text{ MPa}$$

### D3) Flexural resistance

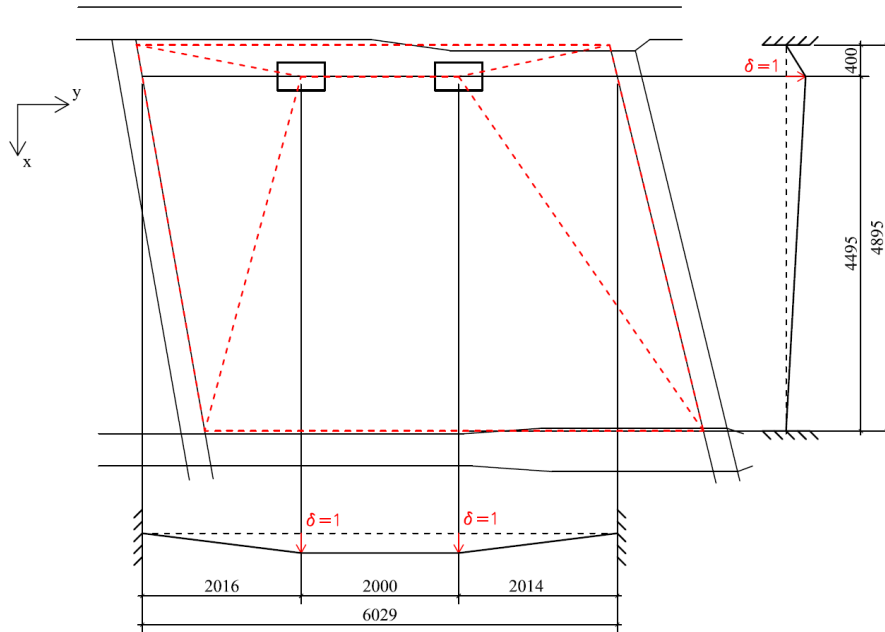


Figure 73: Yield line pattern for fully fixed slab.

Energy conservation principle:

$$Q \cdot \delta = m_{Rd} \cdot L \cdot \theta$$

Where:  $Q \cdot \delta = 2 \cdot Q$

$$m_{Rd} \cdot \theta \cdot L = m_{Rd,x} \cdot \theta_x \cdot L_y + m_{Rd,y} \cdot \theta_y \cdot L_x \quad \parallel m_{Rd} \rightarrow \text{Table 14}$$

x-Direction:

$$m_{Rd,x} \cdot \theta_x \cdot L_y = \left( 181.1 \cdot \frac{1}{0.40} + 37.7 \cdot \left( \frac{1}{0.40} + \frac{1}{4.495} \right) + 183.4 \cdot \frac{1}{4.495} \right) 6.029 = 3594 \text{ kN}$$

y-Direction:

$$m_{Rd,y} \cdot \theta_y \cdot L_x = \left( 135.5 \cdot \frac{1}{2.016} + 46.4 \cdot \frac{1}{2.016} + 46.4 \cdot \frac{1}{2.014} + 135.5 \cdot \frac{1}{2.014} \right) 4.895 = 884 \text{ kN}$$

$$2 \cdot Q = Q \cdot \delta = m_{Rd} \cdot \theta \cdot L = 4478 \text{ kN}$$

Per loading plate:  $V_{Rd} = 2239 \text{ kN}$



Table 20: Flexural resistance at yield joints by assuming a fully fixed support.

Flexural Resistance												
			Reinforcement									
		Sector	Layer	∅ [mm]	gap [mm]	a <sub>s</sub> [mm2]	d [mm]	f <sub>sm,t</sub> [MPa]	b [mm]	f <sub>cm</sub> [MPa]	m <sub>Rd</sub> [kNm/m]	
x-Direction:		1	top	10	220	357						
						16	440	457				
						16	440	457				
								1271	250	584	1000	62.2
		2	bottom	10	270	291	223	584	1000	62.2	37.7	
		3	top	10	220	357						
						16	440	457				
						16	440	457				
								1271	253	584	1000	62.2

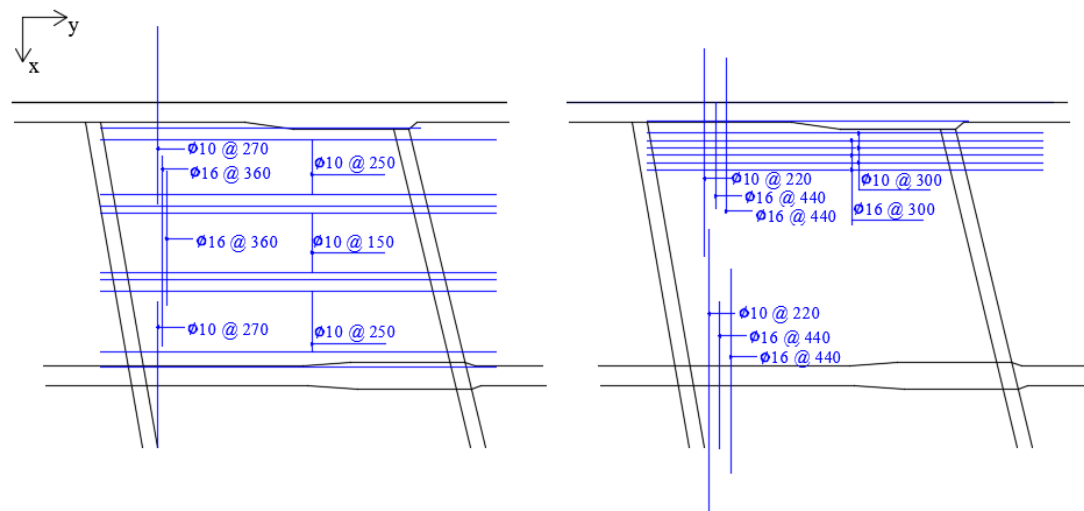


Figure 74: Bottom reinforcement ratio 0.55 % (left) and top reinforcement ratio 0.84 % (right).

## Appendix E – Concrete Properties

### E1) Mean crack distance based on Eurocode 2 (EN 1992-1-1, 2004)

---

Maximum final crack spacing:

$$s_{r,max} = k_3 c + k_1 k_2 k_4 \frac{\phi}{\rho} \quad \text{EC (7.11)}$$

Where:

$$\begin{aligned} c &= 30 \text{ mm} \\ \phi &\approx 13 \text{ mm} \\ \rho_x &= 0.0082; \rho_y = 0.0056 * \\ k_1 &= 0.8 \\ k_2 &= 0.5 \\ k_3 &= 3.4 \text{ (recommendation)} \\ k_4 &= 0.425 \text{ (recommendation)} \end{aligned} \quad \text{Appendix A}$$

$$s_{r,max,x} = 3.4 \cdot 30 + 0.8 \cdot 0.5 \cdot 0.425 \frac{13}{0.0082} = 372 \text{ mm}$$

$$s_{r,max,y} = 3.4 \cdot 30 + 0.8 \cdot 0.5 \cdot 0.425 \frac{13}{0.0056} = 497 \text{ mm}$$

$$s_{r,max} = \frac{1}{\frac{\cos(\theta)}{s_{r,max,x}} + \frac{\sin(\theta)}{s_{r,max,y}}} = \frac{1}{\frac{\cos(0)}{372} + \frac{\sin(0)}{497}} = 372 \text{ mm}$$

$$s_{r,mean} = \frac{s_{r,max}}{1.7} = 219 \text{ mm} \quad (1.7 \text{ recommended factor})$$

---

\* Bottom and top reinforcement considered. If considering only the tensile reinforcement (top reinforcement at the loading area) the value is almost identical since the bottom and top reinforcement ratios are similar.

### E2) Fracture Energy based on Model code (CEB-FIP, 2013)

---

$$G_F = 73 f_{cm}^{0.18} = 73 \cdot 62.2^{0.18} = 154 \text{ MPa} \quad \text{MC (5.1-9)}$$

Where:  $f_{cm} = 62.2 \text{ MPa}$